NTNU
Norwegian University of
Science and Technology

Norwegian University of Science and Technology (NTNU)

The Effects of Speed and Acceleration on the Theta and Delta Band Oscillations in the Hippocampus and Medial Entorhinal Cortex

Master Thesis

Supervisor: Dr. Emilio Kropff

James Eric Sørensen Carmichael

Trondheim, June 20th 2012

Acknowledgements

First and foremost I would like to acknowledge and thank Emilio Kropff for his guidance and advice throughout the course of this thesis. I am very grateful to have had a supervisor that was so willing to share his insight into not only this project but science in general and for taking the time to introduce me to new ideas and methods.

I would also like to thank the entire Moser Lab for providing such an incredible environment in which to learn some of the many facets of neuroscience. In particular I would like to acknowledge the technicians, Kyrre Haugen and Ann-Marie Amundsgård for taking the time to pass on their expertise in building recording drives and performing histological analysis.

Thanks also belong to my fellow students especially, Christin Berndtsson, Annelene Dahl and Martin Wohlwend for their contributions and discussions.

Thanks to Margaret Sørensen for proofreading and correcting this thesis.

I sincerely hope that I will continue my professional association with the faculty, staff and colleagues from the lab in the future.

Finally I would like to thank Shannon Emerson for her support and patience throughout this thesis.

Abstract

The theta band oscillation in the hippocampus and medial entorhinal cortex carries a strong correlation with free movement throughout an environment. Recently several models of these oscillations and their relationship to spatially modulated cells in the hippocampus and entorhinal cortex have started to emerge. One area of focus in theta research has been how the speed of movement modulates the theta frequency. Previous attempts to determine this relationship in the hippocampus and medial temporal lobe have failed to either engage the subject in prolonged running at a constant velocity, or they have not been able to facilitate natural movements during the recordings. Using a novel apparatus that can provide strict control over the speed of a freely moving rat, this study examines the relationship between movement related variables such as running speed and acceleration and oscillations in the theta (7-12Hz) and delta (1.5-6Hz) band in the medial entorhinal cortex and hippocampus during both constant running and during transitions in speed.

The results showed that there was no relationship between running speed and medial entorhinal theta oscillations, as had previously been reported in the open field experiments. Interestingly the modulation of hippocampal and entorhinal theta was related to the magnitude of the acceleration of the animals' movements. This novel finding questions the current opinion attained from open field recordings of instantaneous constant running as well as the models of grid cell firing and theta phase precession that assume a linear relationship between running speed and theta frequency.

Contents

Introduction

"…what makes the brain so special and fundamentally different from all other living tissue is its organized action in time" –*György Buzsáki* *(Rhythms of the Brain, 2006)*

Years of research have identified some of the neural correlates of spatial processing within the medial temporal lobe of the brain. These include cells that react to a certain location, orientation or environmental characteristics, as well as system capable of updating these states based on changes in movement and thus creating a contextual method for navigation that seems to be primarily localized in the hippocampus and parahippocampal region, areas known for their dual role in memory and spatial processing. Though the components for a sufficient memory system seem to have already been discovered, the methods by which these components interact to create a cognitive representation of the world we live in are still being discovered and debated. Moreover the addition of neuronal oscillations capable of synchronizing specific populations of cells, have been shown to be correlated with certain spatial behaviours and seem to play role in the modulation of specific brain systems adds another level of complexity to the matter. To help understand the mechanisms of spatial processing in the brain, it becomes reasonable to perturb some of these modulating forces and assesses the repercussions.

The present study seeks to explore the relationship between constant and changing velocity and the theta and delta band oscillations in the hippocampus and adjacent entorhinal cortex. Past studies have all made use of open field recordings in freely behaving animals or by using running wheels, treadmills or ride-on cars that do not allow for accurate perception of motion by the subject. Alternatively other attempts have been made to assess speed modulation using freely walking subjects which fail to facilitate the manipulation of the velocity of an animal engaged in locomotion and thus cannot achieve accurate recordings of any movement at a prolonged consistent speed. Using a novel technique, this study will track the local field potentials (LFP) of subjects while they are guided by an open bottom cart system allowing for complete control over the exact speed of an animal that is fully engaged in self-motion. Through this experiment we hope to better describe the effects of velocity on self-movement as well as the effects of sudden changes in the velocity of the animal. Prior to addressing the role of oscillations and there potential speed based modulation of spatial processing, a brief description of the anatomy, physiology, behaviour and theoretical implications of the hippocampus, medial entorhinal cortex as well as some of the associated brain structures will be required.

The Anatomy of the Rat Hippocampus and Entorhinal Cortex

The rat hippocampus is located near the caudal end of the brain and spans from near the dorsal surface to the ventral temporal lobes in a C-shaped symmetrical curvature across the two hemispheres (Figure 1A). The hippocampal region consists of the hippocampal formation and parahippocampal region. The parahippocampal region contains the presubiculum (PrS), parasubiculum (PaS), as well as the entorhinal region containing paraentorhinal and perirhinal and entorhinal cortices (EC), all of which contain 6 cell layers. The hippocampal formation contains the dentate gyrus (DG), the hippocampus proper (cornu ammonis (CA) 1, CA2 and CA3 regions) and the subiculum as is outlined in Figure 1B,C (Witter & Amaral, 2004). The hippocampus proper is a relatively unique structure in the brain for several reasons. The first being that it is considered to be archicortical and contains only three cell layers compared to the typical six seen elsewhere in the brain. The amount of intrinsic connectivity within the hippocampal formation also makes this structure quite unique (Andersen et al., 2007). A third defining characteristic of the hippocampus is that the major excitatory projections within the hippocampal formation are mostly unidirectional unlike the more typical bidirectional coupling seen in the neocortex. These first and latter features will be discussed briefly to provide a foundation for discussion of the local physiology and its relationship to spatial behaviour.

The three layers in the DG are the molecular, granule and polymorph layers, while the hippocampus proper consists of the pyramidal cell layer which contains almost exclusively the cell bodies, the cell free 'stratum oriens' and the stratum radiatum which carries into an additional molecular layer (striatum lacunosum-molecular). The subiculum deviates from the other sub-regions of the hippocampus proper in that it contains only two distinct lamina, a pyramidal layer and a molecular layer. The laminar nature of the hippocampus proper plays a critical role in the anatomical allocation of afferent and efferent connections within the hippocampal circuit.

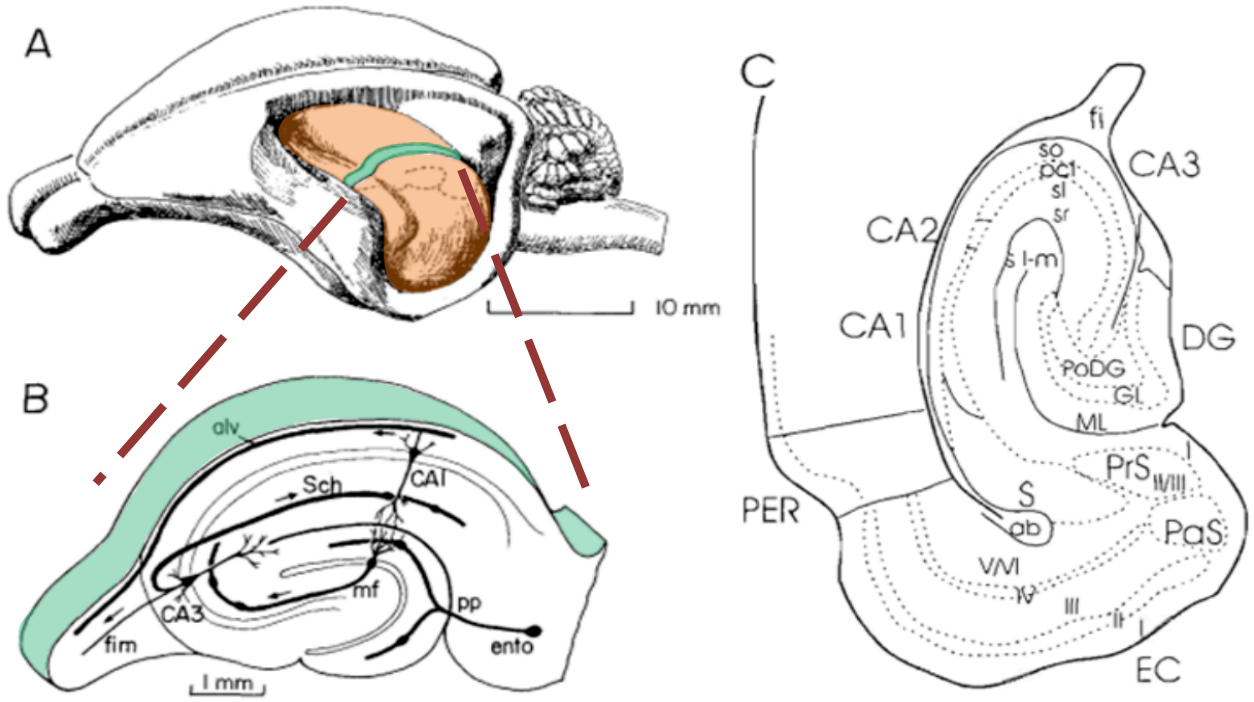

Figure 1: (A) Shows the location of the hippocampal formation in the rodent brain. (B) Shows a simplified schimatic of the major projections in the hippocampus. The perforant path begins in layer II of the entorhinal cortex and projects to the dentate gyrus and CA3 amongst other regions. The dentate gyrus then projects to CA3 via the mossy fibres and from there to CA1 via the Schaffer collaterals, an area also innervated by direct projections from layer III of the entorhinal cortex. The CA1 and subiculum (not pictured) then project to other locations outside the hippocampus, among them layers V and VI of the entorhinal cortex. (C) Displays the specific regions in the hippocampal formation along with the different layers. Beginning in the dentate gyrus we see the molecular layer (ML), granule cell layer (GL) and polymorphic layer(PoDG). The hippocampus proper contains the stratum oriens (So), pryamidal cell layer (PCL), Stratum lucidum (sl), stratum radiatum (sr), and the stratum lacunosum-moleculare (sl-m). Outside of the hippocampus proper we come across the presubiculum (PrS), subiculum (S), and parasubiculum(PaS) before arriving at the entorhinal cortex (EC) and perirhinal cortex (PER) with the angular bundle (ab) running between the PER and CA1/CA2 regions before transforming into the fimbria (fi). (A)/(B) were taken from Andersen et al. (1971), (C) was taken from Witter & Amaral (2004).

Prior to discussing the connectivity within the hippocampus, the anatomy of the entorhinal cortex must first be presented. The entorhinal cortex lies between the parasubicular and perirhinal cortices and is an integral part of the parahippocampal circuit as it is the main input/output region for information transfer to and from the cortical mantle (Andersen et al., 2007). The entorhinal cortex is usually considered to have six layers: four cellular layers (superficial: II, III, and deep: V, VI) and two cell-free (plexiform) layers (I, IV), although the properties of layer IV are currently being questioned. The EC is split into two sub-regions, the lateral and medial cortices which show strong segregations in the connectivity and the associated function. The medial entorhinal cortex is associated with spatial processing spatial information, while the lateral entorhinal cortex is related to sensory information (Hafting et al., 2005;

Yogararsimba et al., 2004)). There is also an extensive level of intrinsic connectivity in the EC with deep layers projecting to the superficial layers and then back to the deep layers. Layer II has been shown to lack excitatory recurrent connectivity while there are abundant pyramidal recurrent connections in layers III and V (Dhillon et al., 2000). The intrinsic connectivity along with some of the inputs and outputs are described in Figure 2 below.

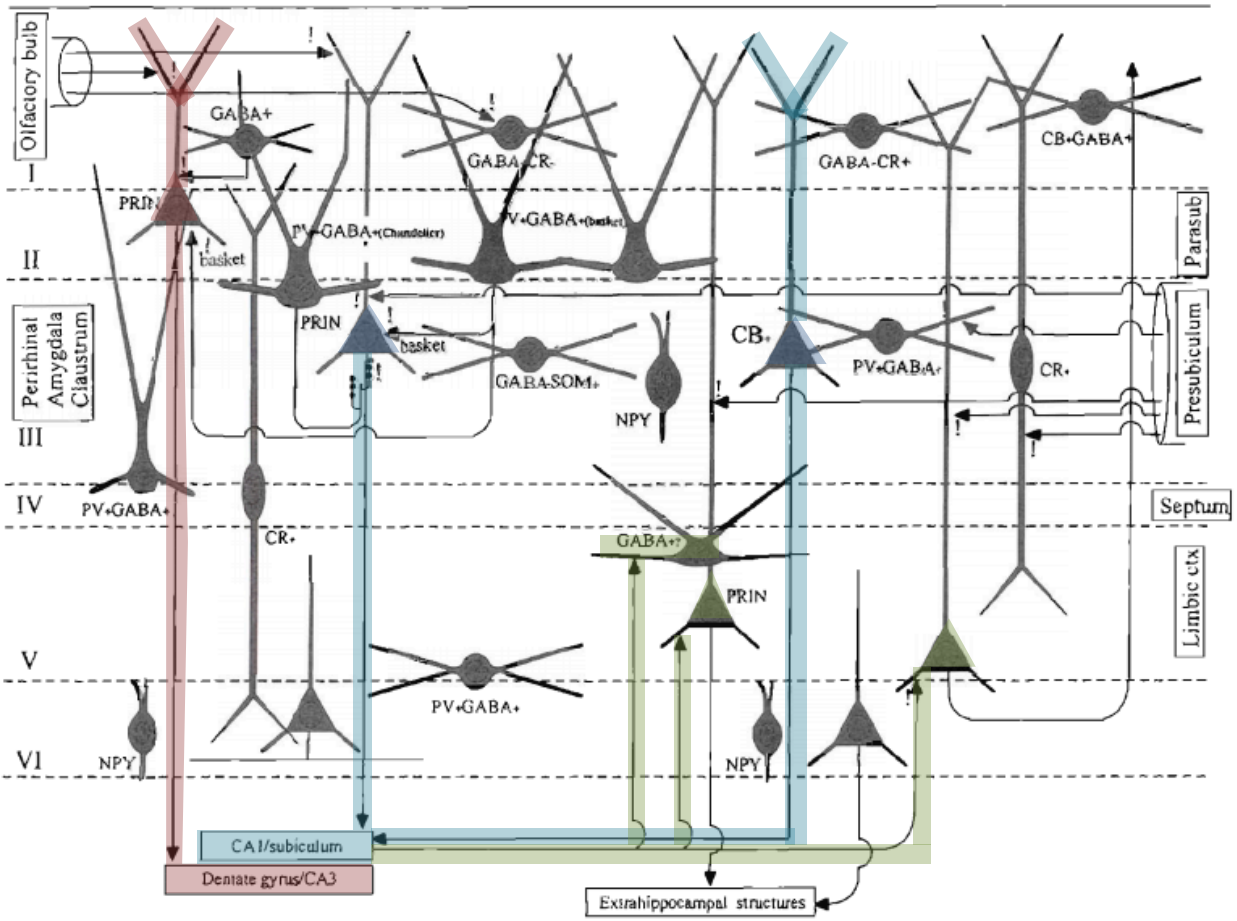

Figure 2: A simplified diagram of the cellular layout of the six layers of the entorhinal cortex as well as the major afferent and efferent connections. The perforant projections from the layer two pyramidal cells to the dentate gyrus/CA 3 region are highlight in red, while the CA1-subiculum output path to the layer V cells in the EC is in green. The second part of the perforant pathway from the layer III pyramidal cells in the EC which project to CA1/subiculum is shown in blue. An adaptation of Wauterlood (2002) in Witter & Amaral (2004).

The main source of cortical input into the hippocampus is via the perforant pathway from layer II of the entorhinal cortex to the molecular layer of the dentate gyrus and to CA3/CA2 (Andersen et al., 1971; Witter, 2007) as well as a second projection from the layer III entorhinal cells to CA1 (and subiculum) (Witter et al. 1988; Leung et al. 1995). There is also evidence of a lesser projection from the deep layers (V, VI) of the entorhinal cortex to the outer two-thirds of

the molecular layer of DG (Kohler 1985; Witter 2007). From the dentate gyrus the granule cells project via the mossy fibres to the proximal apical dendrites of the CA3 pyramidal cells. In addition to the cross region connectivity there is also a high degree of recurrent projections within CA3 (Witter & Amaral, 2004). These CA3 cells then project via coarse Schaffer collaterals which terminate on the apical dendrites of the CA1 pyramidal neurons (Andresen et al. 1971). This connectivity is summarized in briefly in Figure 1B and in more detail in Figure 3.

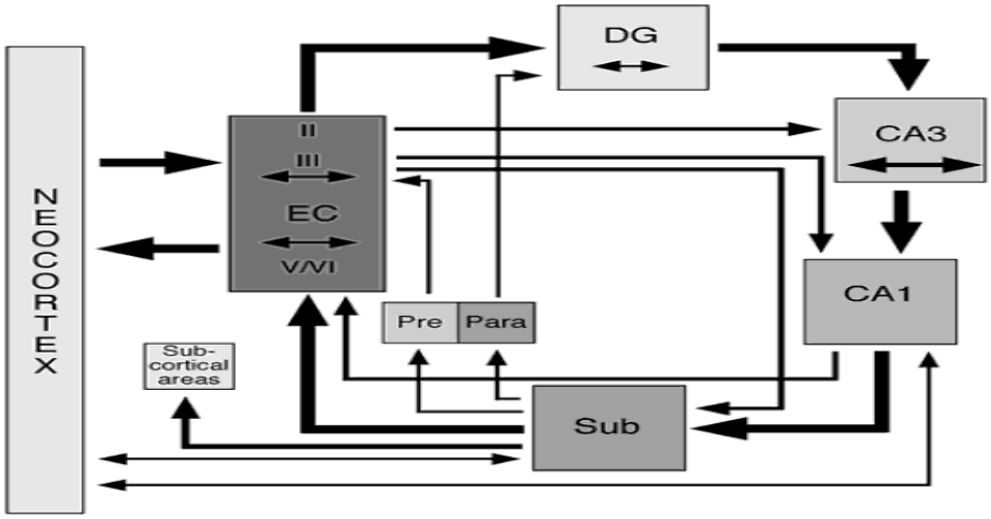

Figure 3: A Summary of the connectivity within the hippocampal formation including neocortical input/output. The principle pathway moves from the neocortex to the entorhinal cortex, then to the dentate gyrus via the perforent pathway. The dentate then projects to CA3 via mossy fibers and then onwards to CA1 via the Schaffer collaterals. CA1 projects to back to the entorhinal cortex primarily by way of the subiculum. This diagram highlights the major unidirectional flow of excitatory activity within the hippocampal formation.

The entorhinal cortex is the main neocortical output while the CA1 and subiculum are responsible for the majority of the projections to the parahippocampal region. Of particular interest to the present study is the specific pattern of reciprocal connections within the CA1-subiculum-entorhinal circuit. Layer III of the entorhinal cortex directly innervates CA1 and subiculum, while the projections from the proximal CA1 and distal subiculum project to the deep medial entorhinal cortex and the distal CA1 and proximal subiculum project to the lateral entorhinal cortex (Tamamaki & Nojyo 1995; Naber et al. 2001; Witter & Amaral, 2004). In addition to the aforementioned excitatory projections an extensive inhibitory system exists within the hippocampal formation and parahippocampal region to facilitate feed-back and feed-forward inhibition, the extent of which are beyond this brief introduction to hippocampal/entorhinal anatomy (for a very comprehensive review of hippocampal inhibitory cells see Freund & Buzsaki, 1996).

Understanding Behaviour through Local Field Potentials

The principle problem in neuroscience is how to extract information about gross behaviours from the anatomy and physiology of the brain. Although a myriad of methodologies exist for studying the actions of neurons, few methods are able to investigate not only the action of specific cells but also the activity of a small population of cells known as the local field potential (LFP). Though the term electroencephalogram (EEG) typically refers to the non-invasive scalp recording technique, it will be used interchangeably with LFP throughout this study. These LFPs are the result of the net changes in the transmembrane potential of all the neurons in proximity to the recording electrode leading to a "mean field potential". The mean field is the summation of the flow of ions from the intracellular space to the extracellular space and vice versa (called "sources" and "sinks", respectively) across all the cells in the recording area since the signals from more distal cells will be lost to the resistance of the closer cells (Buzsaki, 2006) . It is worth noting that the mean field potential is not based only on the cells that reach an action potential, instead it is the much more common excitatory/inhibitory postsynaptic potentials (EPSPs/IPSPs) that have the greater effect on the LFP. The LFP is thus a simplified summation of the collective states of the cells and provides an ideal method for sampling the brain oscillations in a given location.

The Theta Rhythm

The internal oscillations of the hippocampal formation have become a very prominent field of research due to their strong relationship with spatially modulated cells. Of particular interest in navigation has been the theta rhythm that resides within the 7-12Hz spectrum, though this range is loosely adhered to across the literature. Originally described as an 'arousal response' in the hippocampus of the rabbit by Green & Aruini (1954), the 'rhythmic slow activity' as it was historically referred to, was later expanded in 1969 by Vanderwolf. He was able to show that there were changes in theta oscillations in the hippocampus during voluntary movement and not just in other muscular activities such as maintaining posture. Jouvet (1969) was also able to show an abundance of 'slow wave' theta activity in cats during sleep, specifically during the rapid eye movement (REM) phase (Leung, 1984), however the present study will only focus on the motile aspects of the theta rhythm. Despite the high interest in theta associated behaviour, the origin and mechanisms of theta oscillations are still poorly understood.

Before discussing the models of theta generation, a distinction must be made between the two types of theta activity identified by Kramis et al. (1975). The first type of theta rhythm (7-12Hz) is present during 'mobile' behaviours such as locomotion, head movements, and preparation for movement. This form of theta activity is resistant to muscarinic blockers such as atropine and is referred to as type I or 'atropine-resistant' theta. Type II 'atropine-sensitive' theta (4-7Hz) was first described in the anesthetised rat and therefore it was assumed to not be

associated with mobility behaviours. However, it was later shown that type II theta did exist in the awake rat but at a lower frequency during periods of immobile sensory process and arousal, for example during freezing in the presence of a predator (Sainsbury et al., 1987). The atropine sensitivity of the type II theta also suggests that it is modulated by cholinergic input as atropine is a muscarinic acetylcholine receptor antagonist. These two forms of theta rhythms were rarely seen during the same behaviours. Jumping, running, swimming will all produce type I theta while immobility will lead to type II. Vanderwolf (Buzsaki, 2002) proposed type I theta is brought on by the layer II/III entorhinal input into the hippocampus since lesions to this connection wipe out type I theta while type II is still present.

Attempts to discover the source of the hippocampal theta have been focused on the sub-cortical septum. The septum has long been thought to be the central theta 'pacemaker' for the hippocampus and surrounding areas since lesions to the septum, specifically the medial septal diagonal band of Broca (MS-DBB) will abolish theta in the connected structures in the hippocampal formation (Buzsaki, 2002). Petsche et al. (1962) showed a strong correlation between the rhythmically bursting 'B-units' of the MS-DBB and the theta rhythm in the hippocampus by stimulating the reticular efferents (Figure 5). In the same study pharmaceuticals were used to block the hippocampal theta oscillation which led to no changes in the MS-DBB bursting, thus suggesting that this is a unidirectional 'pacemaker'. These MS-DBB projections to the hippocampus are predominantly either cholinergic (excitatory) or GABAnergic (inhibitory). The layer II stellate cells of the entorhinal cortex show a Na^+ based voltage dependant oscillation in the theta range. The inhibitory activity of the septum in combination with the excitatory signals from the entorhinal cortex was thought to create a dipole in the CA1 pyramidal cells (shown in Figure 5). When combined with lesion data during that era this theory became known as the 'classic' model of theta generation. When the cholinergic connections between the MS-DBB and the hippocampus are lesioned there is only a reduction in the hippocampal theta amplitude instead of it being completely abolished, suggesting that the GABAergic projections may be able to sustain the theta activity (Lee et al., 1994). A MS-DBB lesion will extinguish the type I theta in the entorhinal cortex and the removal of cholinergic cells in the MS-DBB will lead to a substantial reduction in the amplitude of the hippocampal theta suggesting that both the cholinergic septohippocampal connections and the entorhinal input to the hippocampus create a seemingly simple circuit for theta generation in the hippocampus (Buzsaki, 2002). The effect of muscarinic blockers on the MS-DBB is mild compared to the removal of these cholinergic projections suggesting an alternative receptor system is likely at work in both the MS-DBB and the atropine-resistant theta generating entorhinal cortex. Buzsaki (2002) points out that amongst other issues, this model cannot account for the variation in the theta phase exhibited by some behaviour such as theta phase precession discussed later in this chapter. Several other caveats related to intrinsic theta generators and the connectivity of the region suggests that there is likely an alternative mechanism of theta generation at work. A second major issue related to the slow timing of cholinergic inputs also sheds doubt on this classic model.

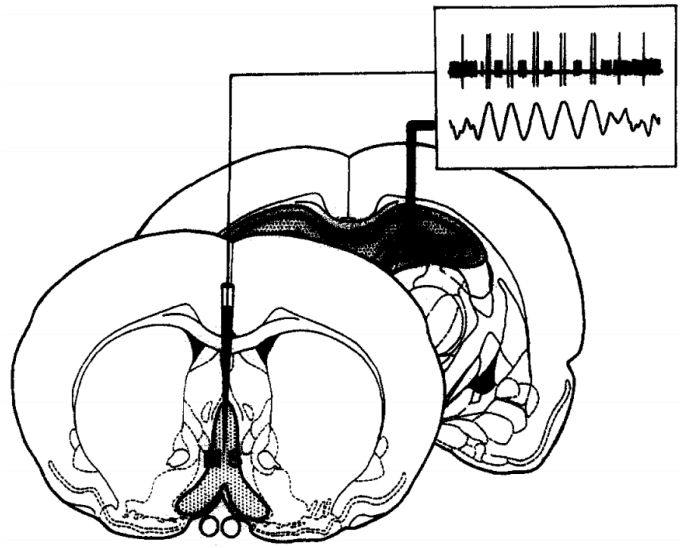

Firgure 4: Shows the location of the medial septal diagonal band of Broca in the forground and the hippocampus in the background. The phase conherence between the rhytmically bursting 'B-units' can be seen firing preferentially at the peak of the hippocampal theta oscillation. Taken from Bland and Colom (1991).

Hasselmo and Fehlau (2001) have been able to demonstrate that *in vitro* addition of either GABA or acetylcholine into the hippocampus produce very different response onset times. The cholinergic inputs had a delay between 1 and 2 seconds which is only in the 1-2Hz range thus too slow to elicit a theta rhythm via directed activation. The GABA input was found to have an onset delay of between 0.2 and 0.7 seconds and can become even shorter based on the duration of the input. The slower direct cholinergic input is unlikely to be responsible for directly imposing the theta band oscillations. Instead the much faster GABA inputs have the potential to sustain theta in the hippocampus. The more likely candidates are the GABAergic inputs, again limiting the likely involvement of the MS-DBB via the cholinergic projections. This does not challenge the classical model but instead puts the emphasis on another component. Over a decade earlier, Bland and Colom (1988) had shown that hippocampal theta could be generated in MS-DBB interneurons. It would seem that by including an intermediate interneuron this would alleviate the timing issue in the cholinergic inputs to the hippocampus.

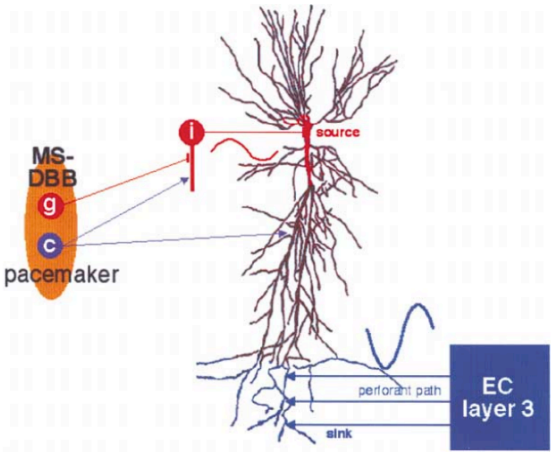

Figure 5: The updated 'classic' medial septal diagonal band of Broca (MS-DBB) pacemaker model of theta rhythm generation in the hippocampus. The GABAergic (g) and cholinergic (c) projections from the MS-DBB control the activity of inhibitory basket cells on the soma of hippocampal pyramidal cells. The entorhinal cortex provides excitatory input to the hippocampal pyramidal basal dendrites creating a dipole with the inhibitory somatic activity. From Buzsaki (2002).

The notion of the MS-DBB being the main source of hippocampal theta is contested by the presence of intrinsic theta generators in the hippocampus. Historically there have been two principle locations of strong theta oscillations in the hippocampus, one in the dorsal blade of the dentate gyrus and the other in CA1 (Winson 1975; Bland & Whishaw 1976). These two theta generators are in opposite phase to one another (180˚) and an inversion of the phase can be seen as one moves their recordings across the hippocampal fissure (Winson, 1975). Bland and Whishaw (1976) saw the most stereotypical rhythmic activity occurred in the pyramidal cell layers of the two generator locations. These hippocampal pyramidal cells have been shown to be capable of intrinsic oscillations via inhibitory post-synaptic potentials in CA1 (Leung and Yim, 1986). Blockage of these CA1 pyramidal cells leads to a massive reduction in the amplitude of the hippocampal theta (Buzsaki, 1990) Taken in conjunction with the aforementioned finding that a lesion of the MS-DBB fails to abolish the hippocampal theta rhythm, this suggests that the intrinsic properties of the hippocampus are more capable than the 'classic' model would imply. King et al. (1998) found that the spetal-hippocampal inputs were rhythmically unstable compared to the robust rhythms of the hippocampus. They further suggest that the septal input could act to entrain the intrinsic rhythm of the pyramidal cells in the hippocampus by setting the frequency and phase and using an updating system rather than a continuous direct activator/inactivator to facilitate hippocampal theta. *In vitro* hippocampal slices will display transient oscillations that contained the theta range (4-15Hz) when carbachol, a muscarinic and nicotinic choline receptor agonist, is added in high enough doses (Bland et al., 1988). Recent studies have found that the application of nicotine to hippocampal slices leads to sharp increases in the frequency but not the amplitude of CA3 neurons which have been proposed to be a source of intrinsic theta oscillations in the hippocampus, suggesting that the α7* nicotinic acetylcholine receptor may be the

alternative receptor system for the type I Atropine resistant theta oscillations (Lu and Henderson, 2010). These findings suggest a strong intrinsic component to the hippocampal theta.

The MEC was shown to be a theta generator by Mitchell & Ranck (1980). They saw that the deep-layers (III-IV) contained the highest amplitude theta and they were in phase with the hippocampal CA1 theta, while in contrast the superficial layers (I) were in the opposite phase to the deep layers making them in phase with the theta signal in the dentate gyrus (DG). Though they did not isolate the MEC from the hippocampus, they were able to conclude that if these oscillations were the result of volume conductance there would be an attenuation gradient in the MEC, which they failed to find. Alonso & Garcia-Austt (1987a,b) were able to replicate these findings in the anesthetized rat. There is a clear phase reversal based on the depth profile of the EC as reported in Hafting et al. (2008) who found that the reversal took place between the EC layer I and EC layer II theta oscillations, a result confirmed by Quilichini et al. (2010). There is also a gradient in the intrinsic theta oscillating frequencies of layer II stellate cells along the dorsal-ventral axis of the MEC (Giocomo, 2007) discussed in detail in later in this chapter.

A strong caveat with research into the source of hippocampal theta is that the majority of the studies use *in vitro* or *in vivo* recordings of anesthetized rats which cannot study type I theta in a naturally occurring manner. Though the connectivity in the hippocampal formation to the MS-DBB is extensive and annihilation of the spetal inputs nearly abolishes theta in this region, the intrinsic properties of cells in the hippocampus and entorhinal cortex suggest that the system is not as dependant on the MS-DBB as once thought.

Lakatos (2005) has shown that a hierarchy of oscillatory control exists amongst the EEG bands in Macaques. They showed that the amplitude of one band is modulated by the phase of the lower frequency and that this is a hierarchical system consistent between bands up to the gamma range. This has been shown in the theta modulated gamma waves seen in layer II/III in the entorhinal cortex (Chrobak et al., 2000) and in the dentate gyrus (Cscicsvari et al., 2003). For this reason the activity in the lower delta band became justified (the power spectrum from pilot data also showed a strong delta component during the cart task, see appendix C).

The Delta Rhythm

Little investigation has been done into the origin of the hippocampal delta rhythm (1.5-5Hz) compared to the much more behaviourally relevant theta rhythm. Delta oscillations have been shown to be an intrinsic property of the thalamus. In the case of decorticated cats, the ketamine induced delta wave is still present in the thalamus but it lacks the bursting properties seen in controls, suggesting that the mechanisms for generating the delta oscillation are localized in the thalamus but they require outside entrainment to create the synchronous bursting pattern (Miyasaka and Domino, 1968). Buzsaki (1991) was able to show a strong thalamic drive in the

pyramidal cells of the cortex specifically via the main bidirectional connection nucleus between the thalamus and the hippocampus, known as the nucleus reunions and the nucleus reticularis. The nucleus reunions has excitatory projections mainly to CA1 with an indirect pathway via the entorhinal cortex layer III (Lisman et al., 2010).

The principle receptor system involved in the generation and maintenance of the delta rhythm is the *N*-methyl-*D*-aspartate (NMDA) which facilitates a thalamo-hippocampo-ventral tegmental loop (Lisman et al., 2010). The addition of NMDA receptor antagonists (in this case ketamine) leads to a hyperpolarization in the activated cells, which activates the T-coupled Ca^{2+} channels leading to Ca^{2+} action potentials with typically very long refractory periods. Ketamine activation of the thalamus leads to activation of the CA1 but not the CA3 pyramidal cells leading to increased firing. This leads to down-stream activation of the ventral tegmental area (VTA) which in turn leads to increased dopamine release in the thalamus via the D2 receptor system. This creates a positive feedback circuit.

Spatial Navigation and the Hippocampal-Entorhinal Complex

Encoding Space in the Hippocampus

After extensive experiments on rats in a series of mazes Tolman (1948) concluded that the brain was not navigating purely based on a stimulus-response system, but instead that the brain was using a complex 'cognitive map', however the anatomical location of this map was a mystery. Following the discovery of movement associated activity in the hippocampus (Vanderwolf, 1969) and the growing evidence that lesions to the hippocampus would impair memory, best summarized at the time by Douglas (1967), the focus of spatial processing research shifted towards the hippocampal formation as the potential source of the illusive cognitive map. The first major breakthrough in understanding the cellular basis of spatial navigation came with the discovery of hippocampal cells that would fire preferentially in a specific location (and sometimes orientation) in a particular environment (O'Keefe and Dostrovsky, 1971). These would become known as 'place cells' due to their preference for one place in the environment and are proposed to be the fundamental unit in Tolman's cognitive map (O'Keefe and Nadel, 1978). Wilson and McNaughton (1993) later showed that the movement of a rat could be predicted based on recordings from a large neural population (73-148 cells) using place cells. They were also able to show that upon entry into a novel environment the spatial representations became much more precise over time.

Place cells have been shown to have several interesting properties related to the transformation of the environment. If an environment is rotated along with all associated visual cues, the place field will follow, however, if only the cues rotate, the place field remains in the same location (Muller and Kubie, 1978). This became known as 'contextual' remapping and was

expanded upon by Jeffery and Anderson (2003) who were able to demonstrate that changing even the colour of the floor could lead to global remapping of hippocampal place fields. These cues do require some time to take effect and create a new map (Bostock et al., 1991). Place field stability has two components, a short-term NMDA-independent phase and a long-term NMDA dependent phase suggesting that the typical mechanism of long-term potentiation and learning are likely involved (Kentros et al., 1998). A second type of remapping occurs when the place fields remain in the same location but change their firing rate, known as rate remapping. These findings show that the place field is not bound to a particular location in all environments and that the context of an environment can have a profound effect on the spatial representation of the environment.

An extremely interesting quality of the place cells is that they have preferential activation with the peak of the hippocampal theta oscillations, a phenomenon known as theta phase precession (Figure 6). The firing of the place cell occurs slightly prior to the peak in theta upon entry into the place field. As the rat moves closer to the center of the place field, the firing becomes one with the peak in theta, then as it leaves the firing drifts away from the peak again ultimately leading to an inter-burst frequency in the place cell akin to the theta rhythm (O'Keefe and Reece, 1993; Burgess and O'Keefe, 2011). The inter-spike interval rate is slightly higher than the theta rhythm and thus leads to the slight step ahead. This activity is more correlated with spatial signals than in time (O'Keefe and Reece, 1993). Currently there are several fields of thought on the cause of this phenomenon, the 'dual oscillator", the "somato-dentritic interference" (not discussed in this study due to incompatibilities with empirical data, see Burgess and O'Keefe, 2011), the "ramping" models, and a network model (Tsodyks et al., 1996) modified by Romani et al., (2011). Only the dual oscillator model will be addressed in this experiment as it claims to be based on the linear speed modulation of the theta frequency, rather than cell spiking.

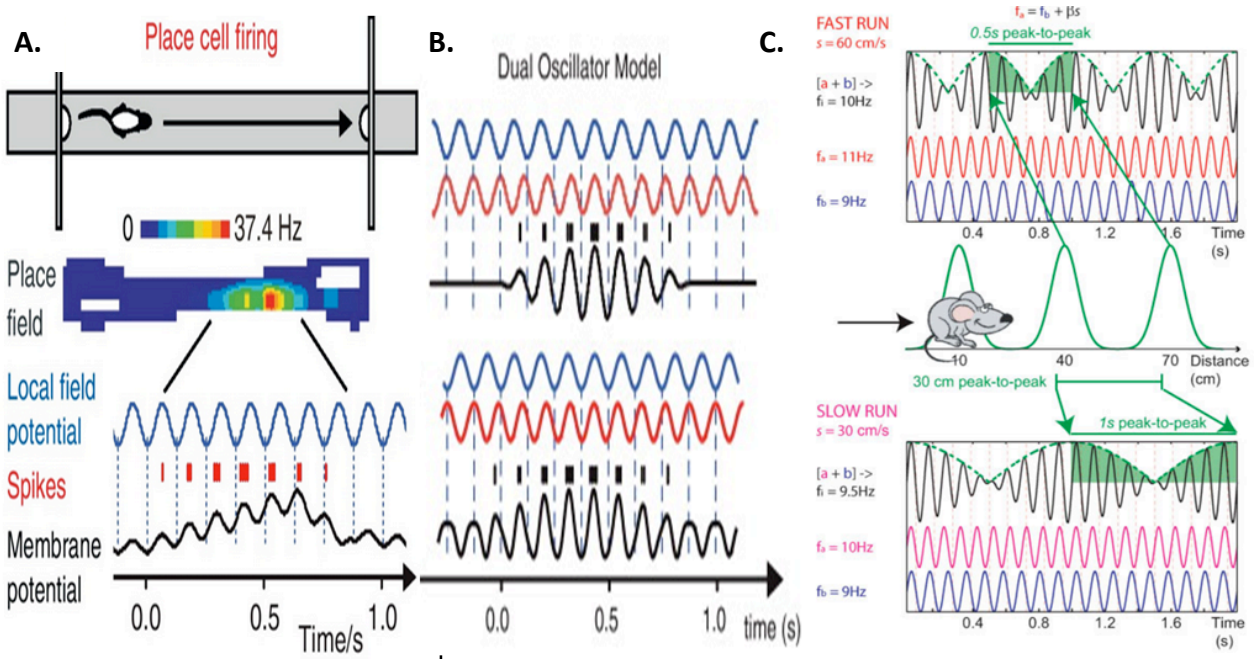

Figure 6: Theta phase precession. **A**) Shows the movement of a rat through a place field and the associated local field potential. The spike bursts are at the peak of the membrane potential oscillation (MPO) and slightly out of sync with the local field potential as the rat enters the place field and by the time they have reached the center, the bursts coincide with the peak in the LFP. As the rat leaves the center of the place field the burst falls out of synch with the peak of the LFP again. **B**) The dual oscillator model of theta phase precession. The upper set shows how two normally asynchronous oscillations can come into phase with one another and produce a summation effect on the membrane potential leading to a signal that is greater than the LFP. This timing facilitates bursts that coincide with the moments in which the phase of the two oscillators are closest to being in phase. When the phases are similar this produces a larger membrane potential and leads to more bursts. The second line shows the same system but instead of an additive effect, the result of phase synchrony is a reduction in the inhibition of the membrane potential. This model uses the assumed linear relationship between the running speed of the subject and the frequency of the dendritic oscillator (the other being the somatic which is more or less in the same frequency as the LFP). **C**) The dual oscillatory model as shown in Jeewajee et al. (2008) showing a clear difference in the summated oscillation between oscillator (a) and oscillator (b). This graphic also shows that the speed of the movement will determine the period of the oscillation with faster movements producing shorter periods. Modified from Burgess and O'Keefe (2011) and Jeewajee et al. (2008).

The dual oscillator model postulates that two oscillations very close in frequency are summed up in the soma, generating an interference pattern. One oscillation is somatic, associated to the theta rhythm, while the other one is independently generated in the dendrites. As suggested by Figure (6C) the interference between two oscillations that are very close in frequency can be thought of as resulting in a fast oscillation, with frequency equal to the average of the two sources, and a slow modulation, with frequency equal to half of the difference between them. The

moments when they are both at peak will lead to a stronger membrane potential oscillation (MPO) (Burgess and O'Keefe, 2011; Figure 6B). This peak would be associated with the center of the place field and thus the moment of highest firing. The extension of the field is controlled by the slow modulation. In the meantime, the fast oscillatory component of the MPO would be at a slightly higher frequency than the somatic source (theta), creating the precession of the place activity with respect to the theta oscillation. It is worth noting that the interference pattern creates not only one but multiple equally spaced fields. When applied to the hippocampus, this model needs an additional mechanism to suppress extra fields (for example through inhibition), but in the subsequent subsection the same idea will be applied in a better fitting situation. Of direct interest to the present study is the relationship between the LFP theta and running speed in the dual oscillator model, which has been assumed to be linear. Only if this relationship is linear, can the temporal slow modulation of the oscillation be transformed into a purely spatial modulation. Should this relationship be non-linear, the system would lose track of position, and the same place field would alternatively appear in different regions of space, depending on exploration.

O'Keefe and Nadel (1978) proposed that the hippocampal "cognitive map" could be based on place cell information, but place cells alone do not suffice as a full representation of the environment (Eichenbaum et al., 1999). The information provided by place cells form a discontinuous and heterogeneous set of points in space and is susceptible to 'clumping' around strong environmental cues. This process is quite good at representing the location of one's self or an object but it becomes difficult to extract information about the relative locations of these things using only place cells. The discovery of grid cells in the entorhinal cortex provides a potential solution to this problem.

Encoding Continuous Space in the Entorhinal Cortex

Research on spatial memory has focused heavily on the different regions within the hippocampus, but it is only recently that attention has shifted to the entorhinal cortex (EC). The two main cortical inputs into the hippocampus come from the medial and lateral entorhinal cortices (LEC/MEC) via the perforant pathway with additional inputs coming from the perirhinal and postrhinal cortices (Amaral & Witter 1989; Witter et al. 1988; Witter et al. 2000). This connectivity led Brun et al. (2002) to abolish bilateral CA3 - CA1 connections leaving the entorhinal cortex as the main source of CA1 activation. They found that the place fields were stable even without CA3 input suggesting that the EC input was sufficient for maintaining the spatial characteristics of CA1 place cells with the only deficits seen in the memories of trajectories and distal locations. The idea that the entorhinal cortex could sustain spatial activity was brought to fruition by Fyhn et al. (2004) who found that there were multi-peaked place-like fields present in layers II and III of the MEC neurons even when the inputs from the hippocampus were severed, showing that there were spatially active cells in the MEC (recordings were also taken from the postrhinal cortex but they failed to yield any cells at this time). The subsequent identification that these MEC layer II/III cells were active in a specific orientation led

to them being called 'grid cells' (Hafting et al. 2005). As the animal moves through the environment the activity of these cells will form a tessellating hexagonal pattern (Figure 7). Subsequent studies have found other spatially modulated cells in the EC such as boarder cells, which are active at edges (Solstad et al. 2008), as well as conjunctive cells with one or more spatial properties, i.e. grid and head-direction (Sargolini et al. 2006) in the MEC suggesting that this region is integral to spatial navigation, but how the system is coordinated with other spatial cells is still under debate (for review see Moser et al. 2008; Zilli, 2012).

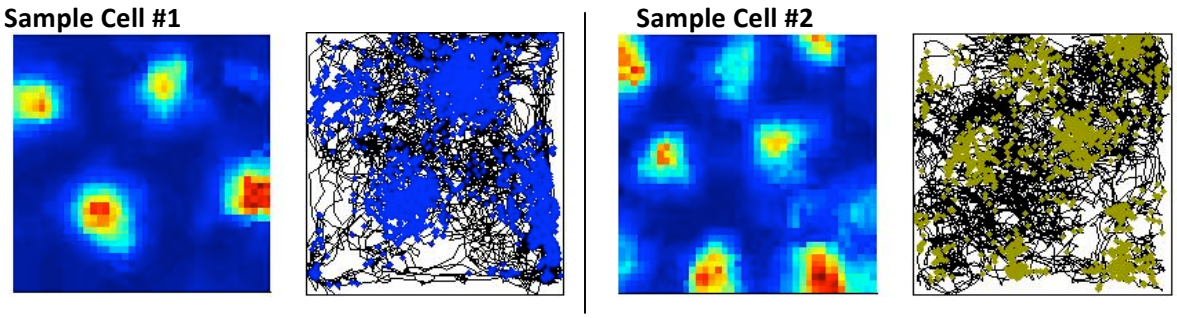

Figure 7: Two examples of grid cells taken from local field potential recordings in this study. The coloured box to the left represent a rate map of the firing patterns of the cells showing activity from blue (no activity) to red (high activity). The right boxes trace the movements of the rats across the environment (black) while the coloured points represent each time a particular neuron fired. The difference in grid scale can be seen between these two grid cells.

There is an interesting correlation between the scaling of grid cells and level of theta modulation along the dorsal-ventral axis (Kjelstrup et al. 2008). This change in grid scaling is similar to the dorsal-ventral gradient of theta resonance frequency seen in the MEC layer II stellate cells from ~8Hz to 4Hz (Giocomo, 2007). Knock out of the hyperpolerization-activated cyclic nucleotide-gated (HCN) 1 channels in the mouse lead to a flattening of these differences in the intrinsic membrane oscillations in MEC layer II (Giocomo & Hasselmo, 2009). The HCN1 knockout mice also showed a perturbation in the scaling of the grid fields in the MEC (Giocomo et al., 2011). Mizuseki et al. (2009) also found a gradient of theta modulation along the dorsal-ventral axis in the EC. They found that the MEC was modulated by alternate theta oscillations, leading to possible activity in the delta band. This finding was replicated and expanded by Deshmukh et al. (2010) who also showed that there was an increase in the relative delta band power, though much weaker than the dominant theta signal, along the dorsal-ventral axis. They hypothesized that the sub-threshold delta oscillations are amplified by the intrinsic 4Hz oscillation (Giocomo et al. 2007) of the ventral MEC neurons which would then lead to strong inference with the theta oscillations and lead to alternate skipping of the theta signal due to the increased probability of firing when the two oscillations were in phase. This result was only supported by a computational simulation and still lacked a generating system for the delta signal, although the prefrontal-hippocampal-VTA delta oscillation seems to likely be a plausible

candidate (Fujisawa et al. 2009; 2011). Theta, and to a lesser extent delta, oscillations have a localized generation and gradient based modulatory effect within the MEC.

When taken in connection with the previous section on the localization of theta oscillations in the hippocampal regions, and the information about the connectivity of the perforant pathway, we see not only an anatomical linkage between the theta generating regions but also similarities in the physiological states of these connected regions suggesting a well define theta system in the hippocampal formation. The extent to which theta oscillations are involved in the hippocampal-entorhinal region can be exemplified in the phase precession seen in grid cells (Hafting et al., 2008).

Head Direction Cells

Prior to discussing the mechanisms behind grid cell dynamics, directional information processing via head direction cells (HD) must first be addressed very briefly. Cells that are responsive to a particular direction in the environment have been found in the anterior dorsal thalamus, the retrosplinal cortex, dorsal presubiculum, and the MEC (Sargolini et al. 2006; Taube, 1995; Taube et al., 1990a; Whitlock and Derdikman 2012). These cells are capable of taking information from the vestibular system, rotational optic flow, and other sensory changes in the angular velocity of the head and convert this to a preferential firing field for a certain orientation (McNaughton et al. 2006). As these cells are more pertinent to the two dimensional models of grid cell firing patterns than one dimensional models, which are not the focus of this thesis, they are only mentioned in passing.

Grid Cell Formation

Since the discovery of grid cells extensive effort has been made to understand what can create such a pattern and how this pattern relates to path integration. The current opinion on the mater typically falls into two major categories of models, oscillatory models and continuous attractor network models. These models can also be categorized based on whether they represent position as two or more independent one-dimensional positions or a single two-dimensional position, known as linear-and planer-coding schemes respectively (Zilli, 2012). Linear coding models use separate information about position and then combine them later on, compared to planar models that use two dimensions to encode position directly. Since the focus of the current study is on the modulation of frequency based on velocity and changes to that velocity, the modern models with velocity dependent variables will be examined in this section, while other velocity independent models will be briefly described or ignored completely (for a full review see Zilli, 2012). For the purposes of this paper only the models that deal with theta frequency related to the running speed of the animal will be addressed in any detail. Some of the other models of interest will only be mentioned in passing.

Linear-Coding Models

The Burgess (2007) oscillatory interference model for grid cell firing is based on the hypothetical ability for grid cells to detect movements of coincidental phase alignment in three or more directionally preferential velocity control oscillators. In other words, if the phases of speed modulated theta oscillations are in phase with one another and each of these signals is offset by 60 degrees in direction, then the hypothetical intersection of these oscillations will produce a grid pattern (Figure 9A,B). This model was then expanded by Burgess again in 2008, with the additional notion that crossing a place field could lead to the phase reset of these VCOs. This newer model was also based on the assumption that the theta frequency shared a linear relationship with increases in the animals running speed (Jeewajee et al., 2008). This assumption becomes integral to the encoding process, because if the theta frequency is not linearly dependant on running speed, the model in its current state cannot compensate for the scaling of distance traveled.

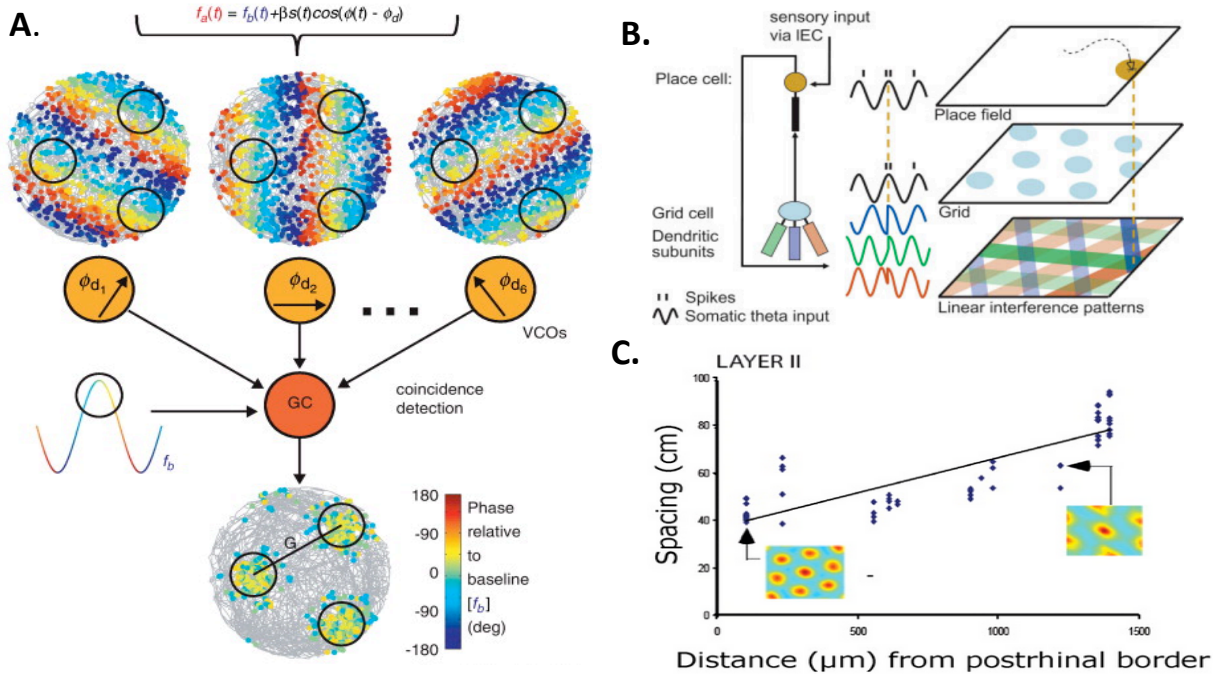

Figure 9: The Burgess (2008) oscillatory interference model for grid cell formation. **A**) The phase synchronization detection of three velocity controlled oscillator sinusoidal waves at ~60˚ from one another by the EC layer II grid cell. **B**) These cells will form an equal lattice based on the angles of the VCOs and thus create a hexagonal pattern of coincidental phase synchrony. The place cell in the upper plane is expected to reset the phase to prevent the accumulation of errors in path integration. **C**) The Giocomo (2007) model based on the grid spacing seen in the dorsal ventral axis. This scaling is based on the changing intrinsic oscillations across the MEC.

Other versions of the oscillatory interference modal offer a similar system with a few minor differences in the assumptions. The model put forth by Giocomo et al. (2007) proposes that the scaling intrinsic frequency of the neurons along the dorsal-ventral axis would act as a regulator of the speed signal and lead to the scaling seen in the field sizes of the grid cells along the dorsal-ventral access (Figure 9C). An issue with the Burgess (2008) model is that the regularity of the baseline is less than ideal for a stable baseline and susceptible to noise. In addition Zilli et al. (2009) were able to create a value for the expected limit for a stable two oscillator stable state. They found that the layer II stellate cells failed to fall within the expected range and thus conclude that the oscillatory models based on spikes and bursts may be idealized (Zilli, 2012). The alternative to the irregular bursting caveat is to treat the oscillations as if they were more realistic rather than treating them as an idealized sinusoid (Zilli and Hasselmo, 2010). By adding noise and other neuronal variables such as gap-junctions they were able to simulate oscillations capable of coupling and producing the grid-like hexagonal pattern.

Alternative to the oscillatory interference model use several other characteristics of spatial cells and coding to explain the emergence of the hexagonal grid pattern. These include using smaller 'theta grids' based on speed modulation to create the hexagonal grid pattern by the moiré interference between theses theta grids (Blair et al. (2007). One alternative is the Navratiloca et al. (2012) model that uses channel hyperpolarization and depolarization to create a 'bouncing' phase precession mechanism that moves from the theta induced precession peak to the synaptic current induced peak behind the firing field in the theta oscillation. A more common method for determining the grid pattern is the use of spike based velocity vectors to create arc measurements from one location to another in time (Hasselmo and Brandon, 2008). There are several other models that are beyond the scope of this experiment yet they provide better insight into the possible mechanisms of grid cell firing, for a review see Moser et al. (2008) and Zilli (2012).

Speed Encoding in the Hippocampal-Entorhinal Complex

Speed and the Hippocampus

As we can see from these models, speed often becomes an important factor in determining not only the formation of grid cells, but also in the understanding of theta phase precession in place/grid cells. For something that seems to be so integral to understanding spatial navigation, there has been a shortage of consistent information on the relationship between speed and the activity in the hippocampal and parahippocampal formation. The current body of literature on the subject is split between two separate but not mutually exclusive correlates of speed modulated neuronal activity. The first being the changes in firing rate in speed modulated cells, and the second as a change in the local field potential across a population of cells. Both forms of speed

encoding will be reviewed here along with the limitations imposed by the current methods used to ascertain the recent data on the subject.

Early studies of the hippocampal theta during running tasks found a somewhat linear relationship between the speed of the animal and the hippocampal theta frequency, amplitude and firing rate (McFarland et al., 1975; in the guinea pig by Rivas et al., 1996; Slawinska and Kasicki, 1998). These studies failed to find a significant difference between the different speeds, thus only suggesting that there is a trend but not an effect of speed on theta frequency. These early experiments were all based on a poorly quantifiable continuous speed and thus they should be treated skeptically as a proof of concept that theta is related to movement rather than running speed having the ability to alter the theta LFP. The true value of these studies is exemplified in the findings of Slawinska and Kasicki (1998) and Rivas et al. (1996) who found a relationship between the firing rate and the theta frequency, although this could be argued as coincidental.

Czurko et al. (1999) used a stationary running wheel to show the relationship between hippocampal CA1 pyramidal cells and interneurons during variable speed running. They found that the pyramidal cells showed a significant increase in firing frequency with increasing positive speed values, while during negative speeds the effect was almost negligible. The interneurons in CA1 show increased firing frequency with increasing absolute running speed. They found that the power of theta were more or less consistent across all speeds. This test does carry the issue of not measuring the activity of a rat engaged in locomotion with all the relevant cues (ie. no optic flow or vestibular signals in the wheel) as well as the problem of extracting data related to constant speed from a highly variable condition.

Maurer et al. (2005) tried to assess if any differences existed in the topography of the hippocampal CA1 in response to speed in an attempt to understand the scaling of place cell fields. They found an increase in the firing frequency in both pyramidal and interneurons with increasing speed in CA1 and that the dorsal CA1 shows a stronger increase in firing frequency than the middle CA1 in both pyramidal cell and interneurons. They did find regional differences in the intrinsic theta frequencies with pyramidal cells having a higher value in the dorsal portion of CA1 than those in the middle. They also found a slight increase in the mean frequency of the theta rhythm in the hippocampus with increasing running speed. Shin and Talnov (2001) also found that while recording from the hippocampus (CA1) there was a negative correlation between theta frequency and decreasing running speed and a positive correlation with increasing running speed. This later study did not look at the differences between the speeds rather just the correlation.

Using different methods for experiencing movement, Terrazas et al. (2005) were able to dissociate various self-motion cues from the firing rate and patterns of CA1 cells. They used a walking condition, a passive moving observation condition (driving a car) and a passive stationary condition in which the environmental cues moved around the animal. In the passive

conditions there was a significant reduction in the firing frequency of CA1 pyramidal cells as well as having enlarged place cells. The theta power was modulated by speed in a near linear manner for the walking condition but the passive conditions produced a nearly flat slope in relation to an increase in speed, as if the rat was still moving but very slowly. These results show that even when certain movement information is removed from the experience, a minimum movement signal is still present.

Speed and the Entorhinal Cortex

In 2006, Sargolini et al. were able to show that the firing rate of grid, head direction and conjunctive head direction x grid cells showed a positive relationship with running speed. The relationship showed a steeper positive slope in the conjunctive cells compared to the grid and head direction cells. These suggest that the MEC spatial cells are capable of updating their firing based on information about the location and any movement signals.

The most recent and prominent example of speed modulating the firing frequency and the mean theta frequency comes from Jeewajee et al. (2008). This study was set up to test the predictions made in Burgess (2008) that the frequency of firing in grid cells over all directions will be dependent on the stationary theta frequency, running speed and the grid scaling. To assess the speed modulation effect, spiking activity and LFP were recorded in the MEC of rats during free running sessions, and from these sessions the data during 20ms epochs of constant running were assessed. They found a strong positive relationship between the running speed and the mean theta frequency which increased linearly at speeds less than 20cm/s and then plateaued for those greater than 30cm/s (Figure 10)

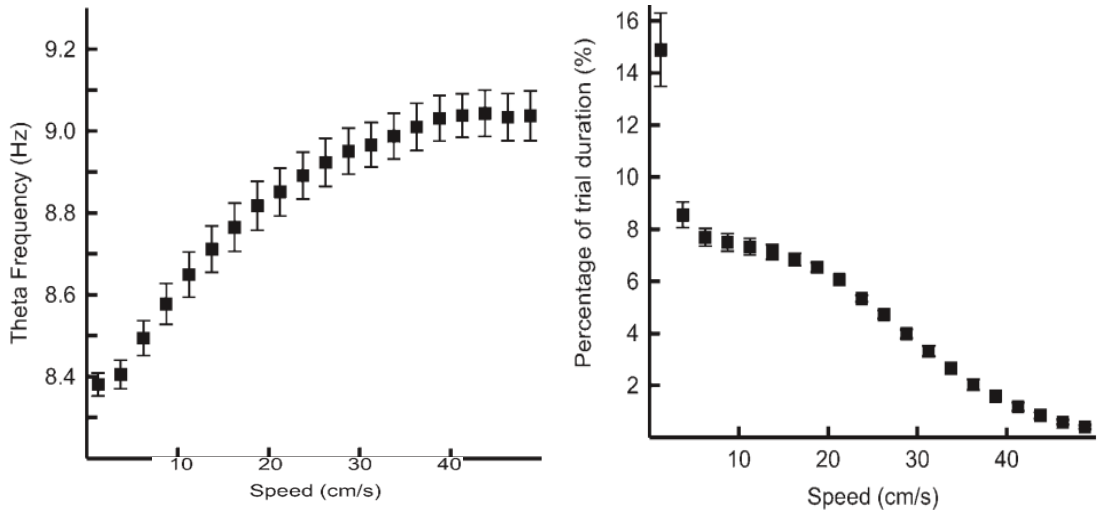

Figure 10: The linear relationship between free running speed and the theta frequency described by Jeewajee et al., (2008). **A**) There is a near linear relationship seen between the ≈5cm/s to 30cm/s. **B**) Thepercentage of each open field session engaged in constant speed running. Taken from Jeewajee et al. (2008).

Aims of this Thesis

As we have seen the spatial navigation system in the brain is a product of specific connectivity leading to a localization of functions correlated with behaviours related to movement and path integration. The specific spatial location encoding place cells, orientation encoding head direction cells, and lattice forming grid cells (amongst others) provide us with the elements required to form a functional representation of space from which ones location and movement can be extrapolated. Several models related to spatial navigation (phase precession, grid cell development, path integration) have proposed that the sensory input from movement speed would allow the system to facilitate an approximate representation of space based on the speed of the animal modulating the theta frequency. The existence of such a speed signal can come in different forms, either as the neural firing rate or through LFP oscillations, which itself could be either a factor in or the by-product of some underlying mechanism. In every case the speed signal is assumed to come from three sources: vestibular, motor or sensory flow cues.

Previous reports on the modulation of spatial cells or subregions have failed to either fully engage the participant in natural movement by using a stationary running wheel (Czurko et al., 1999; Shin and Talnov, 2001), treadmill (McFarland et al., 1975; Rivas et al., 1996), or a moving platform that disengaged some aspect of self-motion (Terrazas et al., 2005). All of these paradigms incur an impedance on one or more of the three sources of speed information. These paradigms would all lead to an inaccurate assessment of the speed modulated behaviour being investigated. The second set of experiments only used data from freely moving rats and lacked a proper control that would allow the disambiguation of speed and other relevant navigation variables such as acceleration (Vanderwolf, 1969; Harper 1971; Slawinska and Kasicki, 1998; Maurer et al., 2005; Grisler et al., 2006; Sargolini et al. 2006; Jeewajee et al. 2008). To correctly examine the effects of speed modulated spatial behaviour, the subject must be able to fully engage with natural movement and have this movement held constant for a long enough period of time in order to formulate any discernible relationship between speed and the LFP.

Current Project

The new apparatus designed by Dr. Kropff allows for the experimenter to strictly control the movement speeds of a rat along a linear track with a variety of environmental cues. By using an open floored cart, the subjects speed can be altered by adjusting the speed of the cart which will cause the subject to engage in normal movement behaviour for the desired speed. Unlike previous experiments this does not hinder the rat's experience of velocity or acceleration. The user programmable nature of the cart system allows for several questions to be answered in a single system.

Hypotheses

The primary goal of this thesis is to better understand the relationship between running speed and the theta and delta band oscillations in the LFP of the CA1 subfield of the hippocampus and medial entorhinal cortex. The previous reports of speed modulated spatial coding either in the theta frequency or the firing rate cells in the hippocampus or MEC have suffered from experimental designs that have not been able to accurately infer a strong relationship between either a rat fully engaged in natural movement or a rat during sustained and consistent running speed. The results from the Jeewajee et al. (2008) report have been used to aid in the formation of models of phase precession and grid cell firing patterns, yet this result is highly sensitive to modulation by other factors than the constant speed due to the instantaneous recordings of speed. Through a better measure of the relationship between the movement speed of an animal and the changes to the hippocampus and medial entorhinal cortex, two areas heavily involved in spatial navigation in the brain, we hope to gain insight into the spatial factors that shape the way the brain processes space.

Secondly this thesis will look at any possible modulation of the hippocampal and MEC theta oscillation during moments of acceleration. This will also examine the effects of the magnitude of the acceleration on the delta and theta band oscillations as well as any effect elicited by the value of the speed prior to a moment of acceleration. Since acceleration is so highly correlated with running speed, it is possible that the results seen in previous studies are erroneously attributing firing rate or theta frequency modulation to moments of acceleration.

Methods

Participants

This study used 11 adult male Long-Evens rats (>3 months old) with an average weight of 475g± 81g. All rats were housed individually in clear plexiglass cages with water being provided ad libitum. The rats were given slight food restrictions (body mass never decreased by more than 10% of their free feeding weight) to encourage foraging behaviour during the open field recording phase and was ceased if the animal freely engaged in foraging. The housing room was kept on a 12 hour light/dark schedule with the recording sessions taking place during the light phase.

All the experimental procedures where approved by the National Research Authority of Norway and all experimenters where a least FELASA C certified. All steps were taken to reduce the number of subjects required and that at no point did the participants endure unnecessary stress or suffering.

Recording Devices

In order to record the local field potential (LFP) in the hippocampal and the entorhinal cells three reconstructed Axona multi-electrode microdrives were used. Each drive provided a possible 16 channels for recording cell activity (48 channels in total). The need for separate recording sites made the smaller microdrive (Axona, UK) the ideal choice compared to other more versatile but cumbersome drive models such as the Neuro-hyperdrive (Kopf, CA), since multiple drives could be placed on the skull of a single rat and still have a sufficient resolution for separating and identifying approximately 5-20 neurons per tetrode (Wilson and McNaughton, 1993).

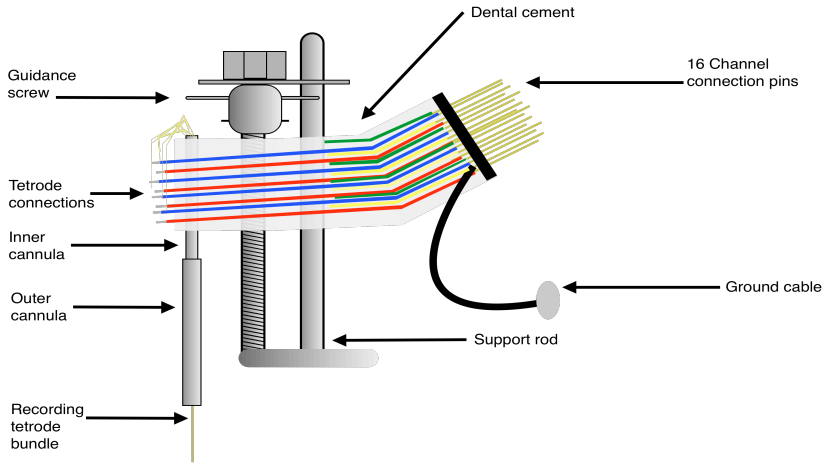

Figure 11: This schematic of a microdrive shows the location and connectivity of all the key components. The coloured lines represent the connection wires for each tetrode. The coloured wires ensured that the electrodes were grouped correctly in order to separate and identify the sources of electrical activity.

The microdrives consisted of four tetrodes. Each Tetrode consisted of four 90% platinum 10% Iridium wire electrodes (California Fine Wire Company #100-167) which have a larger recording range than single electrodes (130 μm and 65 μm respectively) (Gray et al. 1995). Tetrode construction was similar to Gray et al. (1995) with approximately 70 turns/cm and heat bound (2mins at 230˚C). The connection ends of the braided tetrodes were heated to remove the protective coating and inserted into a 23 gauge (.68mm) inner cannula attached to guidance mechanism before being tied to a 17 channel (16 recording + 1 ground) connection piece and secured using "Electro lube" silver conductive paint and a protective coating of nail polish (Chanel No.159) . The guidance mechanism consisted of a moving unit with compression spring wrapped around a stainless-steel screw with a winged nut that would move in 25 μm increments per eighth turn, which was all attached to a support rod. This mechanism was joined to the cannula and connection piece by dental cement (outlined in the above Figure 11). A vertical moving outer 19 gauge (1.09mm) cannula was placed over the inner cannula to protect the protruding tetrode bundles as the drive was lowered over the course of the experiment. The tips of the four tetrodes were cut to the same length to ensure maximum spatial accuracy, electrical sensitivity, and to decrease potential noise from unclean tips. The freshly cut tips were then plated using platinic acid to attain an electrical resistance between 150-300kΩ at 1 kHz.

Surgery

The implantation surgery followed the methods outlined in the supplemental materials to Fynn et al. (2007). The rats were anesthetised using gas isoflorene in a box prior to being placed on the surgery table. Once on the table they were placed in a face mask with 3% isoflorene being pumped into the mask continuously. The isoflorene levels were monitored and adjusted throughout the surgery to ensure that the animal remained in an appropriate state of anesthesia. Once asleep the animals could have their scalps shaved and were then placed in a stereotaxic frame. The skin along the top of the skull was cut and held open prior to drive insertion. Saline was applied to the skull and brain to prevent the tissue from drying or being damaged by the heat of the dental drill. The tetrodes of the hippocampal drive were inserted at 3.0mm right of the midline along the medial-lateral axis (ML), +3.8mm along the anterior-posterior axis (AP), and between 1.6-1.8mm deep along the dorsal-ventral axis (DV). The two entorhinal drives were implanted between4.5-4.8mm along the ML with one on each side and between 1.6-2.0mm (DV). One entorhinal drive was inserted into layer V/VI and the other in layer II/III (the sides would vary from rat to rat). Each drive was grounded using a jeweller's screw secured to the skull. Additional screws with extension pins were also attached and would act as grounds for the recording cables. The drives and screws were fixed to the skull using dental cement and upon completion would weight approximately 13g (2.7% of total body mass).

Following surgery the animals were given 5-7 days to recover. During this time their body weight and health were closely monitored and they were given Metacam (2mg/ml) as an

analgesic. Any wounds were cleaned with saline and talcum powder was applied to the scalp to reduce itching. When the drives were not in use they were bound in tape for protection.

Experimental Conditions

The experiment utilized two recording environments, a 1m x 1m x 0.5m open field box and a 4m x .01m linear track. The open field box was used to identify cells with spatial properties prior to beginning the recordings using the cart system. These cells, which were recorded for purposes beyond the reach of this thesis, served also as a guide to know if the tetrodes were placed correctly inside the regions of interest. In order to track and record the movements of the rats two LEDs were placed on the connecting cables on the head stage of the animal. They were positioned a sufficient distance apart as to allow for identification of head directionality. A camera (Genie model # 8706, with a 2.7-8mm *f*1.0 Computar lens) was placed above the environment. The linear track was set up in a similar manner to the open field with a camera to record the movements and head direction of the rats. A dim desk lamp cast against the lateral wall was used to illuminate the track. The track was elevated approximately 30cm from the ground by two support beams to discourage the rats from jumping off (Figure # A). The track was concealed from the rest of the recording room by a black curtain. Various paper and cardboard visual cues were placed along the curtain and wall adjacent to the track. A second camera was used to track the movements along the track (Ganz model# F11C3, with a 2.3mm *f* 1.6 Computar lens). Due to decreased contrast in the linear track camera, the open field LEDs were replaced by two brighter LEDs on the headstage. Treats (Weetabix "Weetos Choco" cereal or vanilla cookies) were crushed into a fine powder as to avoid any recording artifacts caused by chewing and were scattered across the floor of the box or linear track to encourage movement. The cables connecting the head-stage to the amplifier were counter balanced by a pulley and a weight to minimize obstructing the rats' movement.

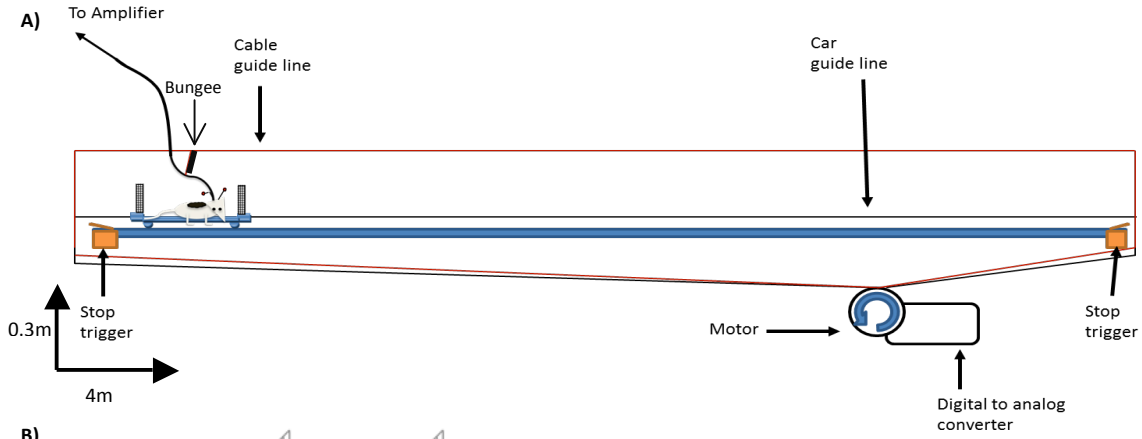

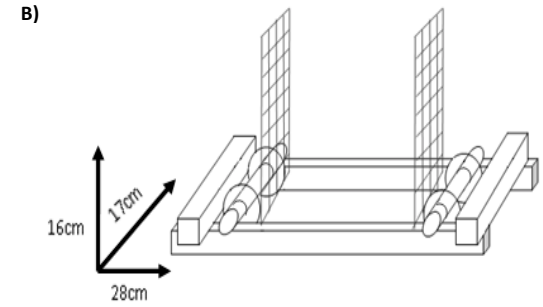

C)

	8cm/s	16cm/s	24cm/s	32cm/s
8cm/s	Constant 0cm/s²	8cm/s²	16cm/s²	24cm/s²
16cm/s	-8cm/s²	Constant 0cm/s²	8cm/s²	16cm/s²
24cm/s	-16cm/s²	-8cm/s²	Constant 0cm/s²	8cm/s²
32cm/s	-24cm/s²	-16cm/s²	-8cm/s²	Constant 0cm/s²

Figure 12: (A) The linear track with the motorized cart. Both the cart guide line and cable guide line are attached to the same motor and thus move at the same speed (B) The dimensions of the cart. Note the open bottom to the cart that allows the rat to walk/run naturally under the guidance of the cart. (C) Table showing the average acceleration for all combinations of prior and new speed. Red signifies negative accelerations, while blue signifies positive values. The purple group are all the stationary running speeds.

The cart was created to guide the movements of the rats along the linear track at specific speeds. The cart was 28cm in length with two ball bearing wheels at each end and supported by rails running slightly below the track along the sides (Figure 12, B). At each end of the car was a wide mesh fence measuring 17cm x 16cm to prevent the rat from moving ahead or behind the car while not obscuring their vision or sensation of velocity. A 25W battery powered motor (Japan Servo) under the track was attached to two sets of guide lines, one to pull the ends of the car, and the other moving a guide wire for the recording cables. By using the battery as an isolated power source allowed for a reduction in the noise caused by AC current (50 Hz) in the wall outlets. Braided fishing line (rated >20lb) was used as the guidance line for its strength, low resistance and lack of elasticity. The cable guide wire had a bungee cord with an alligator clip that would detach if sufficient force was applied to it, thereby reducing the risk of putting strain on the headstage (figure 12, A). The motor was controlled by one of the digital outputs of the recording system via a digital to analog converter (the program is described in the data acquisition section below). At each end of the track there were force-based sensors that would signal the recording system of the cars arrival and thus initiate a stoppage in the motor. During the earlier trials there was a food pellet dispenser at each end, but these were removed in the later trials due to some minor interference with the car and replaced with placing powdered treats at each end by hand. A

kill switch was on hand during the entire recording session that would shut down the motor should anything go awry.

What makes this apparatus unique is that since the cart has an open bottom the rat's movements are entirely their own. The cart serves to guide the speed of the movements while the size of the track allows for only one possible trajectory at a time. Previous studies have never been able to control the rat's trajectory and velocity so precisely without impeding or modifying their natural movements. This self-movement is essential for proper analysis of the theta rhythm as it depends on 'voluntary' movement. After a few training sessions the rats would learn to move with the cart making no contact with the fences at either end essentially creating movements that were completely natural and yet still closely regulated. The curtains along the side of the track aided in this process and appeared to enhance the natural spatial reference frame. Pilot work had shown that without the curtains, the rats would sometimes loose the grid cell maps. This could have been due to a lack of spatial information or a focus on only the cart.

Recording Procedures

Following a full recovery from the implantation surgery, the rats were given a few days of pre-training in the open field. The rat would be placed in the open field without any connection to the recording system and allowed to roam and explore the environment. Food was placed all over the surface of the box to help the animal become more comfortable in the novel environment. This would last between 30mins to 2 hours depending on the behaviour of the animal. During this time the next rat was handled gently by the experimenter to reduce stress during the preparation phase in the coming recording sessions.

Prior to beginning each recording session, the microdrives were connected to the recording system and the gain levels for each channel were calibrated to provide a maximum signal to noise ratio (SNR). If any channels were overly noisy or showed signs of a poor connection, they were grounded. Each open field session was terminated if one of the following criteria was met: if the rat covered a sufficient area as to allow for the identification of different spatial cells, if the cables became detached, or if the program timed out (1 hour). Following the open field phase, the rat was allowed to rest on the preparation stand while the LEDs were switched to the brighter pair.

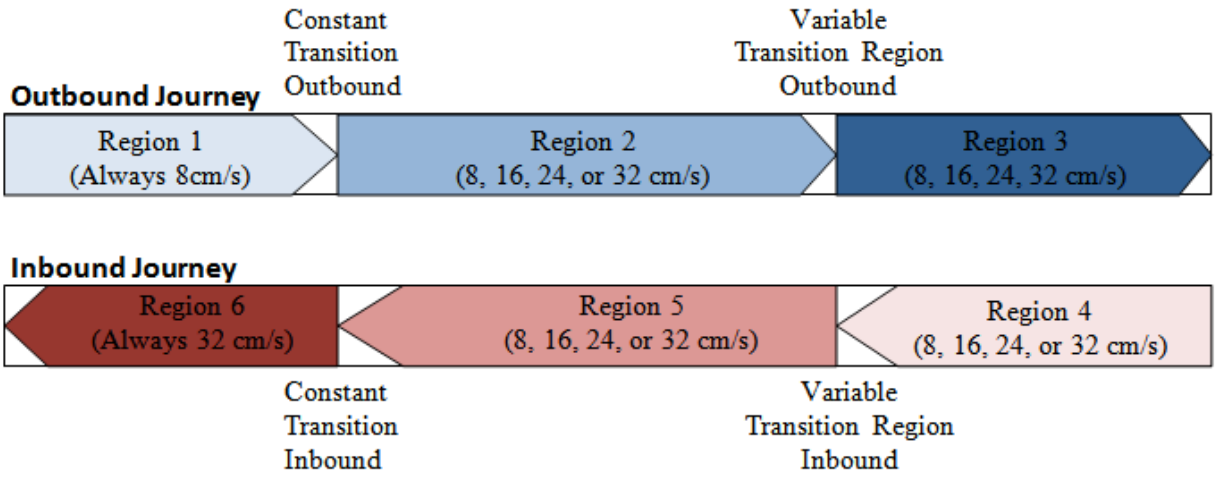

Figure 13: The transition regions and possible speeds within each of these regions. The first transition between region 2 and region 3 (R5 and R6 on the inbound journey) was always at the same location on the track across all trials and all sessions ('consistent transition'). The second transition between region 2 and region 3 (R4 to R5 inbound) would occur within a larger area and would change with each lap ('variable transition area'). The outbound journey would always begin with the 8 cm/s condition. The inbound journey would produce any speed in regions 4 and 5 but region 6 was always 32 cm/s.

In order to study the effect of different velocities and accelerations in the LFP of the rats, four possible running speeds were chosen: 8cm/s, 16cm/s, 24cm/s, and 32cm/s. The transitions between them led to 7 possible mean acceleration values ranging from -24 cm/s^2 to 24 cm/s^2 (Figure 12C). Four speeds were used in order to create a range of velocities that would likely induce noticeable difference in the sensation of velocity of the rat. There is a direct trade-off between the number of conditions and the number of trials needed to procure a statistically viable data set. The smaller number of conditions also allowed for a sufficient number of combinations to be used in each session and while still keeping the duration of the session to a minimum as extended running could cause the rat to tire. The equal distribution in the speeds also allowed for the degree of acceleration to be examined from different starting velocities (i.e. does a change from 8cm/s to 16cm/s have a different effect on the LFP compared to a change from 24 cm/s to 32 cm/s since both are accelerations of 8 cm/s^2?). Pilot data had shown that the positive accelerations were of greater interest than the negative ones, and hence the protocol was designed to favour the positive accelerations. This bias was also used to assess the effect of predictability on positive accelerations by using only values that would elicit a positive acceleration at the start and end points.

Following a successful open field session the rat would then be placed in the cart at the start position and allowed some time to become comfortable prior to initiating the recording protocol. The cart session would always begin at the left end of the track. The control script "eric.bas" was set to twenty laps and then initiated. This program would begin with a loud tone of various pitches (6 seconds in duration) to signal the start of each lap. The rats would quickly

learn to face the appropriate direction upon hearing the cue. Each lap consisted of an outbound (right to left) and an inbound (left to right) journey, each consisting of three velocity regions (1-3 outbound, 4-6 inbound) separated by two transition points (Figure 13). The outbound journey would always begin with an 8cm/s region (R1) and then undergo a transition to the next speed region (R2) at a specific point that would remain constant throughout all the outbound runs for all sessions and for all rats. The speed in region R2 could be any of the four speeds. The transition between region R2 and region R3 would occur at a variable position in the later 2/3 of the track that would change randomly during each lap. The inbound journey would begin with any of the speeds in region R4 before undergoing a transition at a variable location to region R5. The inbound journey would end with a variable transition to 32 cm/s in speed region R6.

The reason that the R1 and R6 regions were held at specific values consistent across all trials was due to the results of the pilot data that suggested that the positive accelerations were producing an interesting finding during positive acceleration. For this reason, if the trial is always started with the lowest value, then there is a higher probability of a positive acceleration occurring during the outbound lap. The same principle is applied to the inbound trial always ending with the highest possible speed. This should render a bias in the ratio of positive to negative accelerations. This could also allow for the analysis of the predictability of a transition in speed since the transitions from R1 to R2 and from R5 to R6 were always held in the same location on the track. This effect of predictability was not utilized during this thesis but it will become an important investigation for future analysis. Upon completion of each lap the rats were given a small amount of crushed food to encourage them to face the correct direction. During the initial car trials a thin line of powdered food was placed down the middle of the track to help guide the rat and to encourage running. To ensure the rats safety the experimenter would walk beside the car to catch it if it fell or became tangled. This was especially important during the first sessions, when rats were not sufficiently accustomed to the apparatus and might try to jump over the fence or out of the track. In case of any incident such as a loose cable the session was restarted from the beginning. If the rat was tired or unwilling to run, something that rarely happened after the first few days of training, the session was terminated and the rat was returned to its cage to rest. Valid sessions included only clean laps with no incidents. Once the laps were completed the car would halt and the rat would be rewarded before being disconnected from the system and returned to its cage.

The rats were fed following each recording session. Sessions were typically 24 hours apart, seven days a week with occasional days off. If a recording session was deemed satisfactory the drives would be lowered 50 μm while the animal was resting in a cloth covered flowerpot prior to being returned to their cage. The recording process would continue until no cells could be identified, typically when the depth of the drives was beyond 4000 μm from the surface of the brain. Once it was determined that the rat no longer had useable recordings, they

were humanely euthanized and their brains were perfused with saline, fixated with 4% formalin, and stored for histological analysis at a later date.

Data Acquisition

The electrical data from the microdrives were passed through a pre-amplifier attached to the input end of the connection cables (Axona, U.K.) which increased the current of the electrical activity in the electrodes of the microdrive several fold. The signal then passed to a DacqUSB amplifier system (Axona, U.K.) where it was coupled with tracking data from the camera and digital input/output signals communicating with the cart. All these signals and the control script were handled by the DacqUSB acquisition software (Axona, U.K.). Because of limitations in the Axona system, channels could be selected either for single unit spike detection or for EEG recording, but not both. The very close proximity of all the 16 electrodes in the bundle allowed for any channel in a drive to be selected for EEG recording, thus selection was based on the quality of a signal at each channel (some variation would exist due to differences in the resistances of the individual electrodes). This proximity also meant that multiple EEG recordings from the same drive would be redundant and thus the remaining 15 channels were used for single unit recording. The single unit data will be analyzed in the future as it exceeds the purpose of this thesis.

The gains for spike detection were set to between 10,000 – 25,000x and a high pass filter of 0.8 to 6.7 kHz was applied (as per Fyhn et al. 2007 supplemental materials). Adjusting the gain allowed for quiet channels that contained useful spikes to be amplified to the point that they reached the threshold for being recorded. Conversely if the signal from a channel was too strong the noise would pass the threshold and thus be recorded, therefore these channels had to have the gain lowered until only the useful spikes were passing the threshold. Noise from the recording areas would contaminate the useful spiking information and thus needed to be removed. To do so a channel with few to no spikes was selected as a reference channel and used to subtract the background noise from the usable signals hidden within.

To record an EEG signal one electrode was selected per drive to be dedicated to EEG recording. Unlike the spike recording channels which used a high-pass filter to remove any lower frequencies, the EEG channels employed a low-pass filter up to 500Hz in order to remove the higher frequency bands. The gain was set to between 1,000 – 2,000x for the EEG recordings. The EEG data was continuously sampled at 4800 Hz during the trial while the spike recordings would only include the data from 200μs prior to and 800μs following the supra-threshold event. An example of the Dacq oscilloscope is shown in Figure 14.

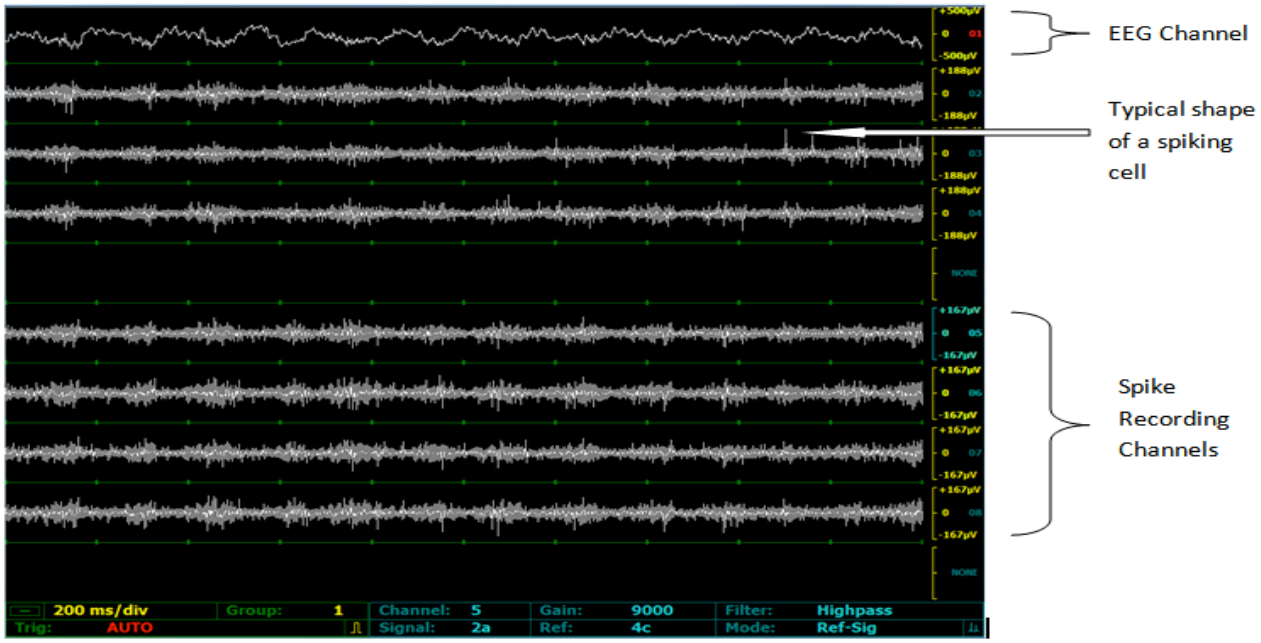

Figure 14: A screen capture of the Axona Daqc digital oscilloscope. Each line represents a channel that corresponds to a single electrode in the Microdrive, grouped in fours to keep each tetrode together. The first represent the lowpass/low-gain (between 1,000-2,000x amplification) EEG channel, which is continuously recorded. This channel shows a prominent theta oscillation. The other channels (2-4, 5-8) are setup as highpass/high-gain (between 10,000-25,000 μV) and require the electrical signal to pass an assigned threshold in order to be recorded. On the bottom row we see that the current channel 5 (group 2, unit 'a') is set to spike recording with the highpass filter and the reference signal being subtracted (Ref-Sig). Notice it is using the third channel in group 4 (channel number 12) as the reference to which this entire group is being compared. The spikes and EEG data are recorded on two separate files.

In addition to the data recorded from the microdrives, a log file was kept that included all the information regarding the changes to the experimental conditions as a result of the program such as car speed, and the start and end of alarm and run periods. Each change was paired with a time stamp relative to the onset of the recording session. This log file would later provide the time frames for analyzing the EEG signals during episodes of fixed speed running or acceleration.

Histology

Once recordings were complete the animal was humanely euthanized in order to verify tetrode location. The euthanasia was carried out using isoflorane (ml/g) gas followed by an overdose of sodium pentobarbital (40-50mg/kg) by intraperitoneal injection. The thoracic cavity of the animal was opened then the blood was flushed with physiological saline via direct injection into the left ventricle of heart. The right atrium was cut to allow all the blood to drain before being fixated with 4% formalin. The electrodes were left in place for 45-90mins before being retracted out of the brain to promote stable fixation and avoid damage upon removal. The skull was then removed and the brain was extracted and stored in formalin (4%) and the microdrives were

removed, cleaned and recycled. 30μm sagittal sections were cut using a cryostat (Microm International, HM 550e), then mounted on gelatin coated slides before being stained with Cresyl Violet (see full protocol in appendix A). The slides were then viewed under a Zeiss AXIO Imager 1 light microscope (Carl Zeiss Microscopy GmbH, Germany) and still images were taken using an attached camera and Axiovision (v. 4.8). The images were then imported into Adobe Illustrator (v.15.0.1) and the contrast and brightness were adjusted to enhance the visibility of the electrode locations.

Data Processing

Following the completion of all the recording sessions, the data from the each trial was compiled with additional information about the date, session type and the depths of each of the mircodrives to create a database of all the pertinent information for each of the participants using Matlab. From this database, two subsets of data were compiled for each of the bandwidths of interest: delta (1.5-6Hz), theta (7-12Hz). The exact frequency of the theta band is inconsistent in the literature, therefore a broad range was used in this study to ensure any strong changes could be accounted for. In particular Vanderwolf et al. (1985) reported instantaneous RSA (theta) as high as 12Hz during sudden or intense movements such as jumping, and since thus study will involve intense changes in movement, the upper band of theta was more liberal than other reports.

In order to analyze the characteristics of the EEG signal it first had to be transformed in order to extract the wave properties such as frequency and amplitude which are essential for this study. The signal was first broken down into its instantaneous frequency for each band width (detla/theta) for each point in time. As mentioned previously this can be done in several manners such as the wavelet transforms, however in this case the Hilbert transform was applied. Pilot analysis found that the information given from the wavelet transform was identical to the Hilbert data but through a much greater degree of down sampling (1/20 vs. 1/4) and thus loss of information. The higher sampling rat in the Hilbert transform offered a better temporal resolution of the instantaneous frequency during a given period compared to the wavelet analysis. For this reason the Hilbert method was preferred. The EEG signal was down sampled from 4800Hz to a less computationally demanding 1200Hz. The signal was then band-passed for the two frequency ranges (1.5-6Hz delta, 7-12Hz theta) by taking the fast-Fourier transform of the signal and removing the frequencies less than the low-cut point (1.5 and 7 respectively) and those greater than the high-cut threshold (6 and 12). The resulting bands were then put through the Hilbert transform, which splits the signal into an instantaneous amplitude and phase. Finally, to obtain the frequency, the phase was unwrapped by adding 2π at each resetting point, resulting in a smooth, monotonically increasing curve. The instantaneous frequency was obtained as the slope of this curve, or in other words, the rate at which the phase advanced. This method of extracting the frequency has been described by Jeewajee et al. (2008).

Unlike the frequency which is independent of the strength of the recorded signal, several factors could alter the amplitude making a method for normalizing the signal essential for proper statistical analysis. The first being that the electrical resistance values were different for each individual electrode meaning that the required gain to produce an acceptable value would be different depending on which electrode was selected for the EEG channel for a given day. The second reason would be that even if the same electrode was used from session to session, the gain would need to be adjusted to cope with the changes in the LFP at a specific location in the cortex. Normalization was accomplished by determining the average amplitude for the most stable condition, in this case running at a constant 8cm/s. Each trial was divided by the median amplitude of the constant 8cm/s components for each drive thus creating a relative value for the amplitude expressed as a percentage of the baseline.

In the event that a trial produced an inferior recording either by movement or contact artifacts, or in the event that a recording cable became detached, a quality value of 0 was assigned to the data for that particular drive and was then excluded during later analysis. In addition to this, several incomplete or invalid trials were identified as problematic during the analysis and were subsequently removed. Two subjects were completely removed from the experiment due to only having one or two training trials. This subject removal process was justified since the excluded participants either had issues with their recording or the location of the recording devices could not be confirmed by the appearance of characteristic spatially modulated cells.

A custom Matlab function was created to identify specific moments in the course of the trial and to extract the time points associated with an event such as a transition. This was accomplished by setting a criterion to be found in the log file (eg: a transition from 8cm/s to 16 cm/s) and extracting the time stamp for that event. A second time was taken which marked the beginning of the next event. This second time was used to mark an end to the prior event to avoid contamination in the signal by, for example, a subsequent transition in velocity. These reference times were then used to take corresponding sections of the frequency and amplitude for the given event. In the case of the acceleration analysis, the band-passed EEG from two seconds prior to four seconds following the onset of acceleration or until the onset of the next transition event. Should a subsequent event fall within the four second EEG section, the points from that reference time until the end of the section would be replaced with null values (NaNs in matlab). The constant velocity data was extracted in a similar manner but instead of the transition events it used the running speeds from regions R2 to R5. These matrices of event based EEG sections were then saved for specific analysis and graphical interpretation.

Statistical Analysis

All statistical tests were carried out using Matlab with the Statistics Toolbox add-on. All the data sets were first put through a one sample Kolmogorov-Smirnov test to determine if the data conferred with an estimated “normal” or parametric distribution based on an estimation from the

sample, in this case using the normcdf (*sample*) function. This test has been shown to be a more powerful alternative to the chi-squared test at all sample sizes and was ideal given the current conditions (Lilliefors, 1967). None of the data passed the test (α=0.05) and thus non-parametric statistics were initially applied to all frequency and amplitude analyses with the exception of the initial attempt to describe the frequency and amplitude during moments of transitions between speeds. This later method was altered due to an unexpected non-parametric trend in the data, explained during the results section.

Stationary Running Periods

As outlined in the previous sections the track was split into an outbound (R1, R2, R3) and an inbound (R4, R5, R6) lap. Each lap consisted of two transitions; one held constant between R1 to R2 and R5 to R6 while the other would vary across the later 2/3 of the track. Each lap had three possible speeds and two regions were always constant (R1=8cm/s, R6-32cm/s). Throughout these trials a large sample of all the constant velocities emerged. The runs sections included any time that the rat maintained a constant speed one second prior to or two seconds after a jump occurred. The constants speed sections were put into three categories: start, end and run. The start and end conditions were cut in order to remove any accelerations associated with movement initiation or cessation. To analyze how different constant velocities could influence theta and delta oscillations, sections of the LFP recording were created for the two cortical locations in which the rats were moving at a constant velocity. Paired- sample statistical analysis requires that each data point have a corresponding partner and will result in an error if they are incomplete. This was done by identifying the conditions (either the hippocampal or MEC datasets) that were incomplete and removing the entire trial from the analysis. The Friedman non-parametric analysis of variance was applied to test for differences across the velocity conditions while taking into account the trial by trial trends, roughly equivalent to the repeated measures analysis of variance (ANOVA) used for parametric data (chapter 5 in Sprent & Smeeton, 2000). The confidence interval values were determined using the Bootstrap method since it has been shown to be one of the best genuinely nonparametric estimators of statistics compared to other methods such as the Jackknife (Efron, 1981). This method uses an extremely large hypothetical data set based on the actual values in the real data (in this case, hypothetical n=100,000) to estimate not only the standard error but also the confidence intervals based on both the percentile and bias corrected and accelerated percentile (default Matlab function "bootci").

Transition Periods

Each acceleration period was split into several categories in order to conduct proper analysis of the variables of interest. Response epochs and were extracted on a trial-by-trial basis (outlined in figure 15). The response region included the quarter second immediately following the acceleration. By taking all these six second sections of the accelerations within each lap it was possible to perform statistical tests of the different acceleration values on the different oscillations by comparing the response epochs to those of a baseline value, in this case the no change

transitions of the same prior speed. This comparison was chosen since the difference should be equivalent to the difference between acceleration and a constant velocity.

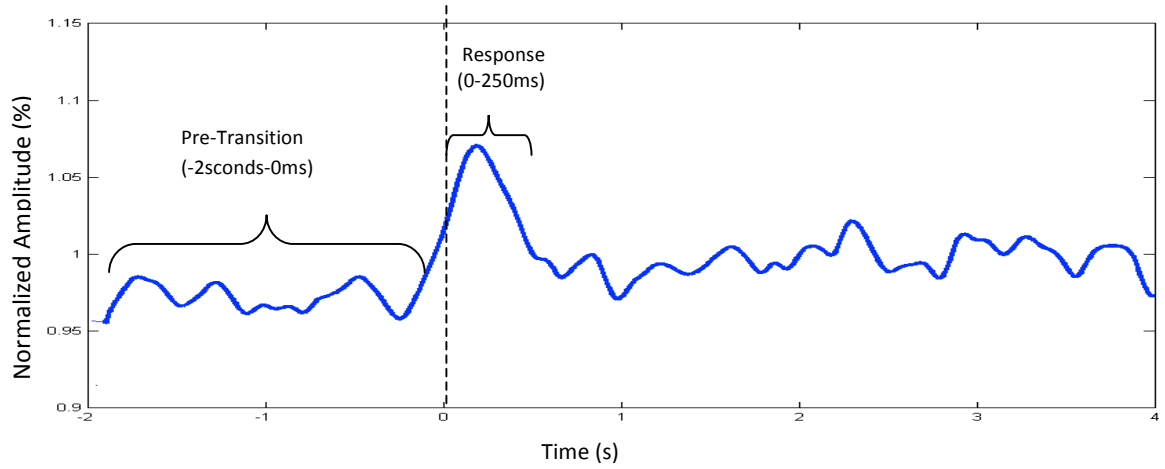

Figure 15: Shows the location of the sections created in order to analyze any acceleration induced changes in the LFP. The pre-transiotion epoch consisted of the 2 seconds leading up to the transition (labeled 0 in the x axis) while the transition epoch contains all the data points from the onset of the acceleration up until 250ms afterwards. This image is a smoothed example of the theta amplitude surrounding an acceleration.

In order to test the effect of the magnitude of the acceleration on the theta and delta oscillations, the acceleration conditions with the same net acceleration value (ie. 8cm/s to 16cm/s, 16cm/s to 24cm/s and 24cm/s to 32cm/s are all accelerations of $8cm/s^2$). To quantify any effect of the degree of acceleration the median values during the response epoch were compiled and the distributions of these sets were compared to the other accelerations in both positive and negative cases using a Kruskal-Wallis non-parametric analysis of variance with a Bonferroni post-hoc analysis of the differences between groups. A similar method was applied to test for the effects of the prior speed on the response from the transition in speed. Instead of compiling the acceleration conditions, they were instead tested within the same acceleration conditions for any differences in the response based on the magnitude of the initial speed prior to the transmission. The same Kruskal–Wallis analysis was applied.

Results

Histology

Verification of the tetrode location was done during the experiment by identifying the characteristic theta oscillations or cells with spatial patterns typical of the target region (place fields in CA1 and grid cells in MEC layer II/III). These were verified after the perfusion of the brain using 30micron slices and staining them with Cresyl-Violet. In one case (rat #16365) the hippocampal drive was positioned slightly towards the CA2 region. In order to be included in the analysis the drive needed to show the theta rhythm and it contained some place modulated cells, and thus it was kept in the full analysis. Examples of the two recording locations from rat #16347 are shown here (Figure 16). The Rat Brain Atlas (Paxinos and Watson, 2007) was used to verify the location of the hippocampal drives. The atlas was limited in how far it went in sagittal slices to the lateral edge, therefore an in-house atlas was used to identify MEC sites.

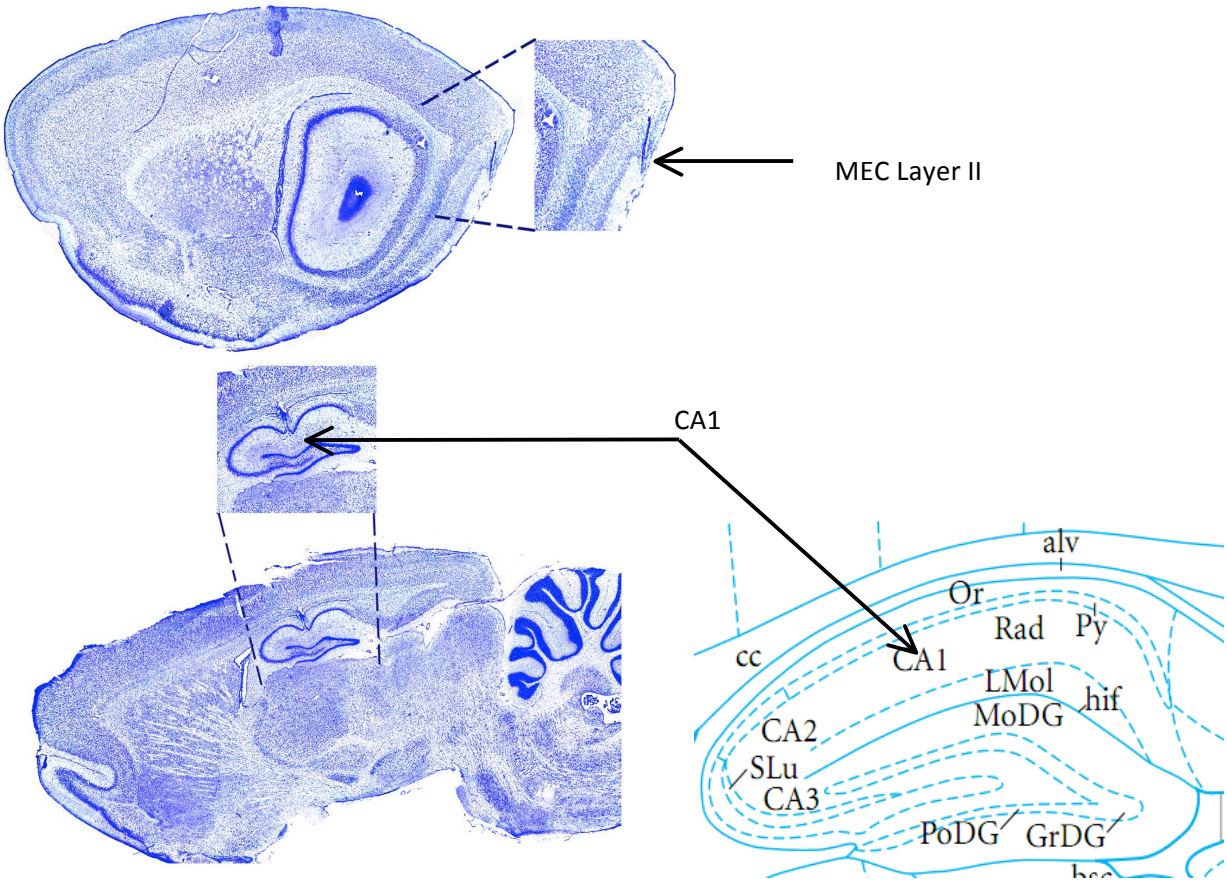

Figure 16: Tetrode conformation by Cresyl Violet staining. The upper panel shows an MEC layer II tetrode tract. The lower image on the left is of a CA1 tract while on the right is the corresponding index taken from the rat brain index (Paxinos and Watson, 2007).

Stationary Running Periods

The term stationary is used here in the sense of a system that is constant over time; hence the running speeds being investigated are stationary in that they are invariant for extended periods. The relationship between theta frequency and the running speed of an animal has been used to explain phase precession and the formation of grid cell firing fields. Previous studies reporting such as relationship have been limited, and no previous method of measurement has been able to either fully engage the animal in movement or been able to sample constant speed effectively. For this reason the stationary running speed of the rats in the linear track under the guidance of the motorized cart will be analyzed to provide a better understanding of any relationships between theta frequency and stationary speed.

Data from the cart sessions were split into six sections (Figure 13 in the previous chapter). Sections 1L and 6R were removed due to only having one set velocity (8cm/s and 32 cm/s respectively). All the running periods of constant velocity (2L, 3L, 4R, 5R) within the four remaining regions were pooled for statistical analysis. The data sets failed the Kolmogorov-Smirnov test of normality and since non-parametric tests utilize the median as a point of comparison rather than the mean, non-parametric tests became ideal due to the irregularity/bias in the data. Due to the limited set of velocity points the more common linear regression analysis reported for wheel (Shin and Talnov, 2001) or open field analysis (Jeewajee et al., 2008) would not have been useful. Instead the non-parametric Friedman test of variance was implemented to determine if any effect of velocity could be found on the median frequency at either of the recording sites.

The Friedman analysis failed to find a statistically significant difference between the median frequency values across the four velocities in the medial entorhinal cortex ($\chi^2(3)=2.72$; $P=0.44$; Figure 17B) This is in stark contrast to the positive relationship seen by Jeewajee et al. (2008) and questions the proposed properties of the VCO. The Friedman analysis did find a significant difference in the hippocampus, however no discernible trend emerged, contradicting the correlation seen in Shin and Talnov (2001) ($\chi^2(3)=42.92$; $P=2.56\text{x}10^{-9}$; Figure 17A). A Bonferroni post-hoc comparison found that the difference occurred between the 8cm/s and 24cm/s conditions only. This lack of effect questions the current models built around a VCO component. We show a variation between 7.95 - 8.05 Hz compared to the 8.4 – 9.1Hz seen in the Jeewagee et al. (2008) finding.

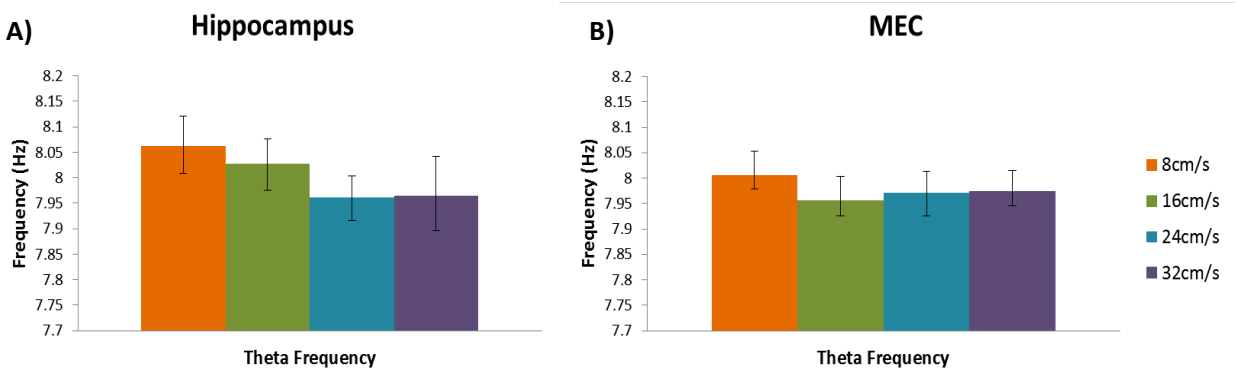

Figure 17: The frequency of the theta signal during the four different constant velocity conditions in the hippocampus and MEC (median ±95% confidence interval). (**A**) The values of the theta frequency in relation to the running speed at the hippocampal recording site. The only difference across the conditions was found between the 8cm/s and the 24cm/s velocities. (**B**) The frequencies seen in the MEC recording site. No velocities were able to elicit a significant difference in the median theta frequency.

The delta band oscillations were analyzed in the same manner and found a significant difference across the median frequencies in the hippocampus ($\chi^2(3)=55.36$; $P=5.74\text{x}10^{-12}$; Figure 18A). There was also a significant difference across the four speeds in the MEC ($\chi^2(3)=124.85$; $P=6.97\text{x}10^{-27}$) which showed a potential trend towards a negative relationship between velocity and delta frequency (Figure 18B). However, Bonferroni post-hoc comparisons found that the difference in the frequency of the delta signal in both the hippocampus and MEC was only noticeable in the 8cm/s condition compared to the other higher velocities. The lack of consistent differences across the speed conditions renders any inference of a trend to be little more than speculation.

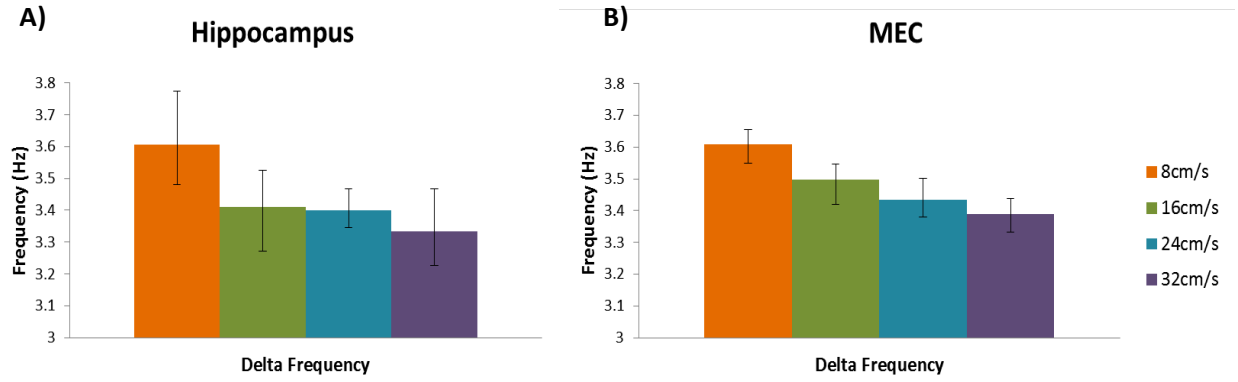

Figure 18: Delta frequencies across the four possible velocity conditions (median ±95% confidence interval). (**A**) The hippocampus showed a clear difference between the 8cm/s condition and the upper two velocities. (**B**) The MEC displayed a similar relationship with the 8cm/s condition being significantly higher than all three other velocities.

To determine if this effect of velocity (or lack thereof) was limited to only the frequency of the hippocampal and MEC oscillations, the amplitude of the theta and delta signals were also analyzed (summarized in Table 1). The theta amplitude only showed a significant difference in the MEC ($\chi^2(3)=44.65$; $P=1.10\text{x}10^{-9}$) between the 8cm/s and 32cm/s conditions, while the hippocampus failed to show any difference in the median amplitudes ($P>0.05$; Figure 19A, B). The 8cm/s velocity had a lower median amplitude in the MEC. The delta amplitudes were found to be different in both the hippocampus and MEC, but instead the 8cm/s median amplitude was greater than the median amplitudes at higher speeds ($\chi^2(3)=16.99$; $P=7.11\text{x}10^{-4}$; $\chi^2(3)=40.15$; $P=9.9\text{ x}10^{-9}$ for each recording area respectively).

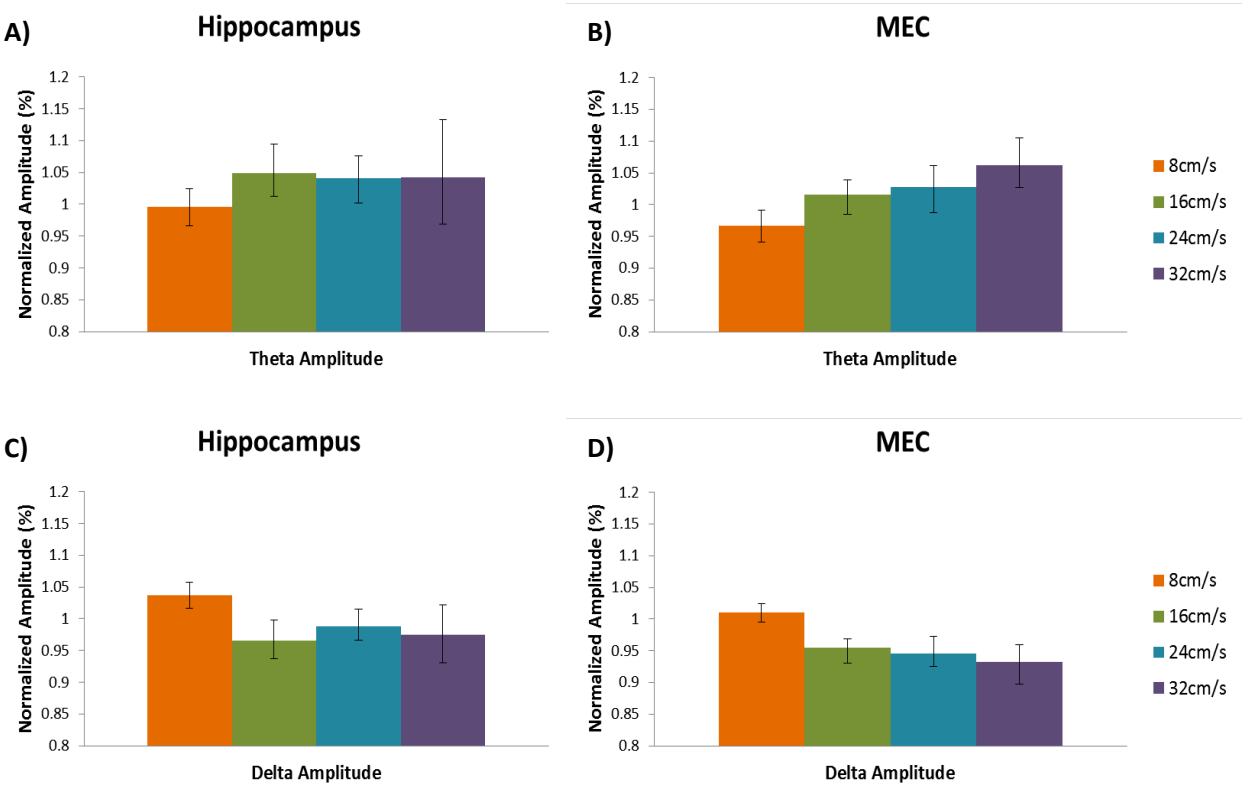

Figure 19: The normalized amplitude of the theta and delta band oscillations in the hippocampus and MEC during periods of stationary velocity (median ±95% confidence interval). **A**) The hippocampal theta amplitude shows no significant changes across the four constant velocities. **B**) The 8cm/s velocity has statistically lower amplitude than the upper three speeds in the MEC suggesting a potential positive relationship between running velocity and theta amplitude. **C**) The delta amplitude is higher at the lowest speed than at the three higher velocities in the hippocampus. **D**) The 8cm/s condition is significantly higher in the MEC and then shows an opposite trend compared to the theta amplitude with a decrease in the amplitude as the velocity increases. All amplitudes have been normalized by the 8cm/s condition.

TABLE 1: Summary of the Analysis of the Constant Running Speeds

Theta Frequency	Hippocampus	MEC
Friedman Analysis	$\chi^2(3)=42.92$; $P=2.56\text{x}10^{-9}$	$\chi^2(3)=2.72$; $P=0.44$
Cross Speed Differences	8cm/s vs 24cm/s	N/A
Delta Frequency		
Friedman Analysis	$\chi^2(3)=55.36$; $P=5.74\text{x}10^{-12}$	$\chi^2(3)=124.85$; $P=6.97\text{x}10^{-27}$
Cross Speed Differences	8cm/s vs 16cm/s, 24cm/s, 32cm/s	8cm/s vs 16cm/s, 24cm/s, 32cm/s
Theta Amplitude		
Friedman Analysis	$\chi^2(3)=4.61$; $P=0.20$	$\chi^2(3)=44.65$; $P=1.10\text{x}10^{-9}$
Cross Speed Differences	N/A	8cm/s vs 16cm/s, 24cm/s, 32cm/s 24cm/s vs 32cm/s
Delta Amplitude		
Friedman Analysis	$\chi^2(3)=16.99$; $P=7.11\text{x}10^{-4}$	$\chi^2(3)=40.15$; $P=9.90\text{x}10^{-9}$
Cross Speed Differences	8cm/s vs 16cm/s, 24cm/s, 32cm/s	8cm/s vs 16cm/s, 24cm/s, 32cm/s

Analysis of LFP Oscillations during Transition Periods

When conducting the analysis of the effects of transitions in speed (acceleration) on the LFP, the moments of accelerations themselves could be isolated and treated as individual events allowing for concatenation across all the laps, sessions and rats. For this reason the acceleration analysis need not treat the individual accelerations in a pairwise manner (as had been done in the analysis of constant velocity). This increased the sample size up to three orders of magnitude compared to the constant speed analysis since trials with missing values could still include the data from the useable recordings (example: a missing hippocampal recording would not exclude the one from the MEC). Kolmogorov-Smirnov tests were applied to the acceleration data finding that none of the data sets conformed to the normal distribution. The data sets were then manually inspected using a histogram plot. The distribution suffered from a small and consistent skew favouring the most common frequency from the Hilbert transform in the filtered range for both theta and delta bands (≈8.1Hz and 3.5Hz respectively). The very large sample size and consistency of the skew in the data sets allowed for the application of parametric tests to non-parametric data by invoking the central limit theorem. However, initial application of the parametric tests revealed a large occurrence of type I errors due to the skew of the data set. For this reason the non-parametric Wilcoxon rank sum test was applied to comparisons between two samples and the Kruskal-Wallis test was used for tests involving three or more samples.

To properly address the effect of acceleration on the theta and delta band oscillations, three properties had to be quantified. The first being the degree to which the values of the LFP changed as a result of the acceleration. This was analyzed by applying Wilcoxon rank sum test

(α=0.05) to compare the median values of the different transitions to a baseline value set by a constant speed transition equal to the prior speed (eg: 8cm/s to 16 cm/s were compared to the transitions from 8cm/s to 8cm/s). The result of this comparison would determine if there was a significant effect of acceleration on the amplitude or frequency of either the theta or delta oscillations in the two recording locations. The second measure was to determine if the magnitude of the acceleration could have a scaling relationship with any changes in the frequency or amplitude. This was assessed by comparing the three net acceleration values during the post transition peak (0-250ms) using a Kruskal-Wallis test and applying a Bonferroni post-hoc comparison to assess for any inter-group differences. It is worth reiterating that though there were six possible positive changes in velocity, these were collapsed into net acceleration conditions, i.e. 8cm/s to 16cm/s and 24cm/s to 32cm/s are both accelerations of 8cm/s^2. The results of the comparison of the magnitudes of acceleration on the LFP would determine if the effect was modulated by the intensity of the acceleration or alternatively that any acceleration passing a detection threshold would induce a universal response in the LFP at a particular recording location. A similar process was used to determine the third property, seeing if the velocity prior to the transition would elicit a difference in the transition induced response. The accelerations were categorized based on the pre transition velocity (ex: 8cm/s to 16cm/s could be compared against transitions from 16cm/s to 24cm/s) Again Kruskal-Wallis tests were applied to the accelerations of 8cm/s^2 while the Wilcoxon rank sum test was applied to the two 16cm/s^2 accelerations. Finally the Bonferroni Post-hoc comparisons were used to determine the differences across groups.

Theta Frequency during Acceleration

A positive change in velocity was observed to consistently produce a very sharp increase in the theta frequency in the MEC as well as the hippocampus. This increase in the speed resulted in a 'typical' transition induced response in the frequency predominantly during the first 250ms after the moment of acceleration. Figure 20,21 shows the clear and consistent peak in the frequency brought about immediately following a positive acceleration, the data across all positive and all the negative transitions were pooled here for clarity. The change in theta frequency during the 250ms following the acceleration was quantified by subtracting the baseline theta frequency seen in the no acceleration transitions of the same prior speed (Table 2). The significance of these changes was assessed with the Wilcoxon rank sum tests, the results are also summarized in Table 2. Taken in conjunction we can see in these tables that the positive acceleration values will elicit a significant sudden increase in the theta frequency in both the hippocampus and the MEC during accelerations greater than 8cm/s^2, and in the case of transitions from 8cm/s to 16cm/s. Taken in conjunction with the findings in the previous section these results suggest that it is not the magnitude of the velocity, as suspected in previous studies, that modulates the frequency of the local theta oscillations in these two areas but instead the rate at which the velocity changes in time.

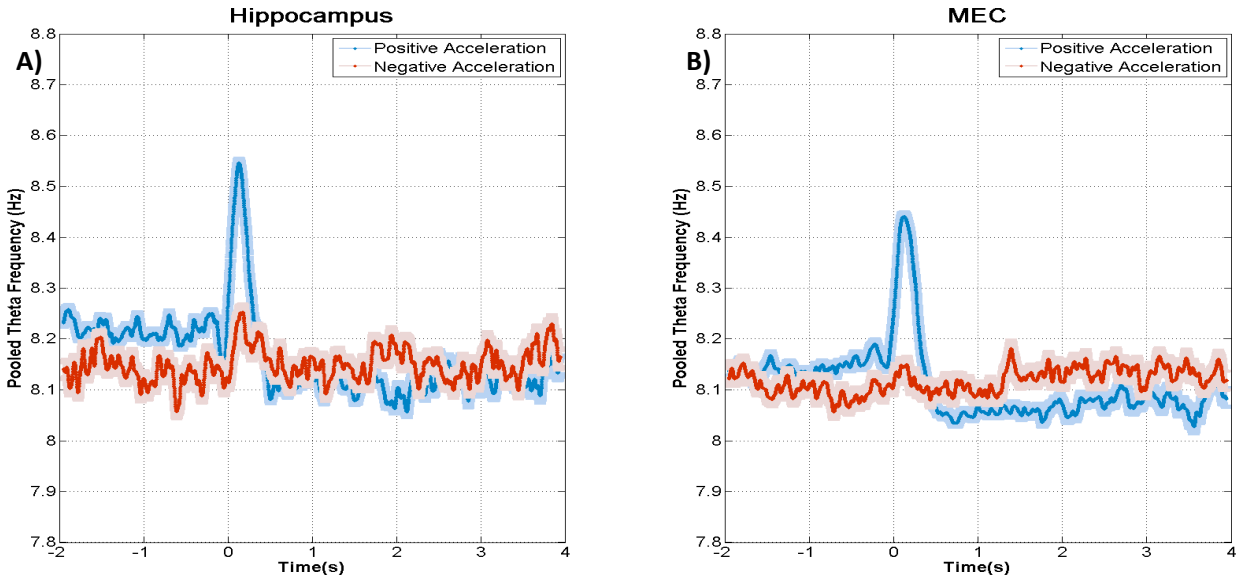

Figure 20: The acceleration induced peak in theta frequency. This graph shows the median of the pooled data from all the positive (blue) and negative (red) accelerations across all trials and subjects (±SEM in lighter colours). The peak seen in the theta frequency immediately following the transition will be referred to as the 'typical acceleration peak' through the remainder of this study. **A**) The hippocampus shows a clear peak in the theta frequency during positive accelerations and a minor increase in the frequency during negative conditions immediately following the transition in velocity (addressed in the following chapter). In the positive transitions the frequency appears to continue to be lower following the peak, however the frequency does return to roughly the same value as the pre transition period with time (not shown in these plots for clarity). **B**) The MEC shows a similar peak following the transition to higher velocities however; unlike the hippocampus the negative acceleration does not show a peak at the point of transition. Like the hippocampus the trough does return to the pre-transition values.

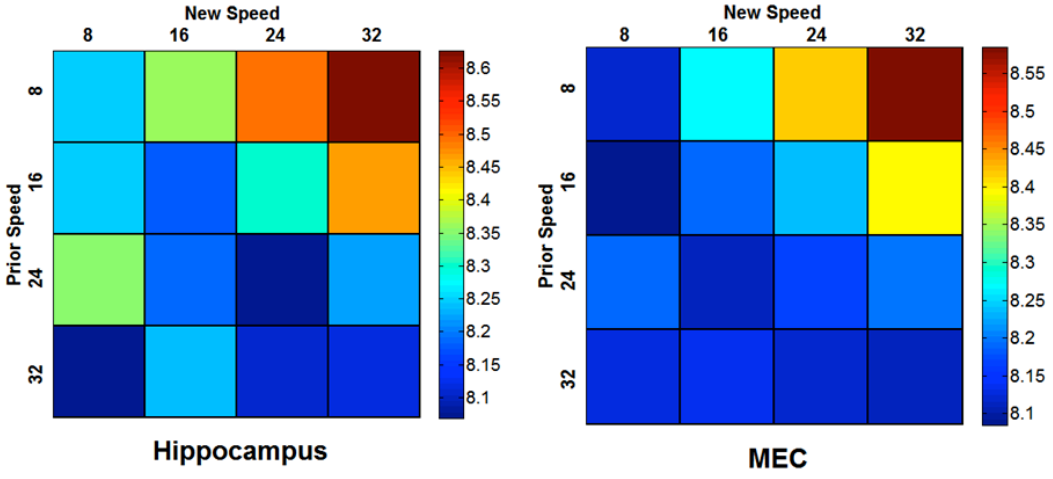

Figure 21: Heat plots of the median peak in theta following a transition to a new speed. Both plots show a much higher theta frequency in the 250ms following the transition. The value of the theta frequency at the peak increases with the rate of acceleration in both the MEC and hippocampus. The hippocampus shows that nearly all negative accelerations will not produce a frequency at the peak that significantly differs from the baseline levels, with the exception of the 24cm/s to 8cm/s and 32 cm/s to 16cm/s transitions. The MEC displays no significant differences between the baseline theta frequency and the frequency as a…

Figure 21 continued:…result of negative accelerations while showing a strong relationship between the increasing positive acceleration and increasing peak frequency.

TABLE 3: Difference in Theta Frequency (Median Peak – Baseline in Hz)

Hippocampus

Prior Velocity \ New Velocity	8 cm/s	16 cm/s	24 cm/s	32 cm/s
8 cm/s	0.00	0.15**	0.21***	0.36***
16 cm/s	0.07	0.00	0.18	0.31***
24 cm/s	0.14*	0.03	0.00	0.03
32 cm/s	-0.04	0.20*	0.03	0.00

*(P<0.05), **(P<0.01), ***(P<0.001)

MEC

Prior Velocity \ New Velocity	8 cm/s	16 cm/s	24 cm/s	32 cm/s
8 cm/s	0.00	0.15***	0.30***	0.46***
16 cm/s	-0.11	0.00	0.00	0.18***
24 cm/s	0.09	-0.04	0.00	0.03
32 cm/s	0.00	0.02	0.02	0.00

*(P<0.05), **(P<0.01), ***(P<0.001)

The differences between the acceleration transitions and the baselines outlined in Table 3 show that all the transitions to higher velocities have a progressive increase in the theta frequency, suggesting that the magnitude of the acceleration may have an effect on the magnitude of the theta frequency response. The transitions to lower velocities lead to no statistically significant changes in the frequency with the exception of the 24cm/s – 8cm/s and 32cm/s – 16cm/s conditions, which were found to produce a significant increase in the theta velocity in the hippocampal recording area.

All the transitions with an equal net change in velocity were concatenated into three groups for the positive and negative accelerations (-24 cm/s^2, -16 cm/s^2, -8 cm/s^2, 8cm/s^2, 16cm/s^2, and 24cm/s^2). This allowed for an analysis across the net accelerations using the Kruskal-Wallis non-parametric test of variance to determine if the pure magnitude of the acceleration was modulating the change in the theta frequency (the medians of the change values are displayed in Figure 22). The magnitude of the acceleration produced a significant difference across the hippocampal and MEC theta frequencies (H=92.29, 2 *d.f.,* $P=3.71\text{x}10^{-21}$, H=261.37, 2 *d.f.,* $P=1.75\text{x}10^{-57}$ respectively). The Bonferroni post-hoc comparison found that the median theta frequencies in the transition period were significantly different between each of the three acceleration magnitudes at both recording sites. There was no effect of the magnitude in the negative accelerations in the MEC (H=5.08, 2 *d.f.,* $P=0.08$). There was a difference in the three negative accelerations in the hippocampus (H=10.60, 2 *d.f.,* $P=5.00\text{x}10^{-3}$) but the post-hoc

comparison found the difference to be inconsistent with the increasing magnitude of the acceleration with the -16cm/s^2 group leading to a higher median theta frequency than the -24cm/s^2 group. The strong relationship between the increasing magnitudes of positive accelerations suggests an alternative to the previously postulated velocity modulation of MEC/hippocampal theta frequency, with acceleration producing a scaling increase based on the rate of change in velocity only when going to higher velocities.

To test for any possible modulatory effects of the velocity prior to transition on the acceleration-induced peak in the theta frequency in the MEC and hippocampus, comparisons were made between the values of the change in frequency. This was done by using a Kruskal-Wallis test of variance on the three 8cm/s^2 acceleration conditions (8cm/s-16cm/s, 16cm/s-24cm/s, 24cm/s-32cm/s) to see if the starting velocity would have an effect even though the acceleration value is the same. This test found a difference in the hippocampal and MEC theta frequency in the three variants of the 8cm/s^2 acceleration (H=19.7, 2 *d.f.,* P=5.27x10^{-5}, H=15.96, 2 *d.f.,* P=3.00x10^{-4} respectively). The Bonferroni post hoc comparison found the only differences to exist between the 8cm/s to 16cm/s and the 24cm/s to 32cm/s conditions, which were then confirmed and quantified using a Wilcoxon rank sum in the hippocampus (H=3.96, 1 *d.f.,* P=7.63x10^{-5}) and MEC (H=3.96, 1 *d.f.,* P=7.63x10^{-5}). A Wilcoxon rank sum test was used to test for differences in the median theta frequency in the 16cm/s^2 acceleration variants (8cm/s-24cm/s, 16cm/s-32cm/s). Neither produced a significant effect on the local theta frequency in the hippocampus (H=0.5, 1 *d.f.,* P=0.48) or the MEC (H=1.02, 1 *d.f.,* P=0.31). No differences were seen in the theta peaks during negative accelerations across different prior speeds. These results remove the possibility of velocity modulating the acceleration-induced peak in the theta frequency in the hippocampus and MEC, leaving the magnitude of the acceleration as a potential candidate for a creating a scaling effect. The -8cm/s^2 acceleration does follow the same trend as the +8cm/s^2 acceleration in the hippocampus. This could be due to the increased lateral movement of the head at lower speeds and accelerations since the velocity of the cart is not taking the full attention of the rat and they are looking around the environment. The lateral acceleration of the head could trigger this slight modulation.

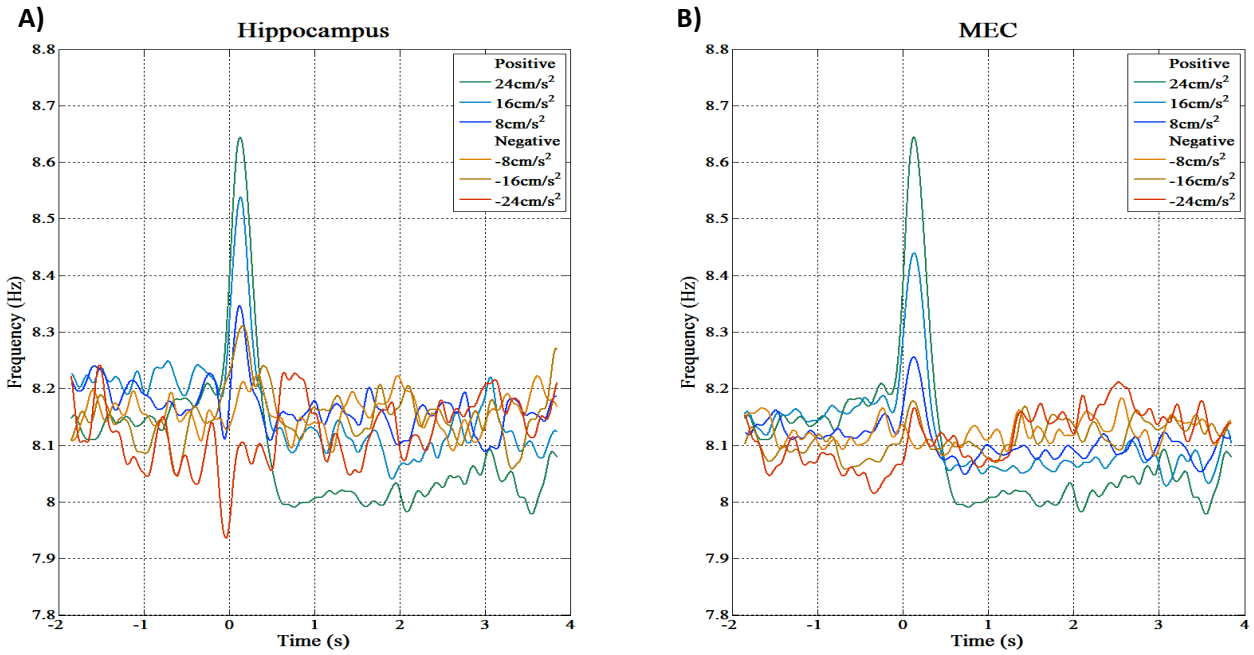

Figure 22: The effect of the magnitude of acceleration on the theta frequency. In each case the transitions were broken down into groups with the same net acceleration. **A**) Shows the separation of the positive acceleration conditions based on the degree of acceleration. This follows a progression with the greater accelerations leading to higher peaks in the theta frequency. As seen in Table 3, there is an unusual peak in the -16cm/s^2 condition in the hippocampus compared to other negative conditions across both sites. **B**) The MEC shows a very clear separation based on the rate of acceleration. All three positive accelerations produce statistically significant different increases in the theta frequency, while the only group difference seen in the negative conditions is between -8cm/s^2 and 24cm/s^2. All values represent the median across all moments of acceleration recorded for each condition.

Delta Frequency during Acceleration

The frequency of the delta rhythm did not yield the acceleration peak seen in the theta range. Instead the delta frequency followed the trend seen in the previous section where increases in the speed lead to a decrease in the frequency and vice versa (Figure 23). This effect was particularly clear in the MEC compared to the hippocampus (Figure 23 A, B). A Wilcoxon rank sum analysis of this transitional trend failed to consistently yield a significant difference in the frequencies between the accelerations during the 250ms peak compared to the baseline zero acceleration conditions across all the transition variants (Table 4, Figure 23). There was a consistently significant decrease in the frequencies in the transitions from 8cm/s in the MEC. This trend was not clear in the hippocampus. In contrast, the transitions from a higher to a lower speed would elicit an increase in the frequency. However this was inconsistent and rarely significantly different than the baseline transitions to the same speed as the prior speed.

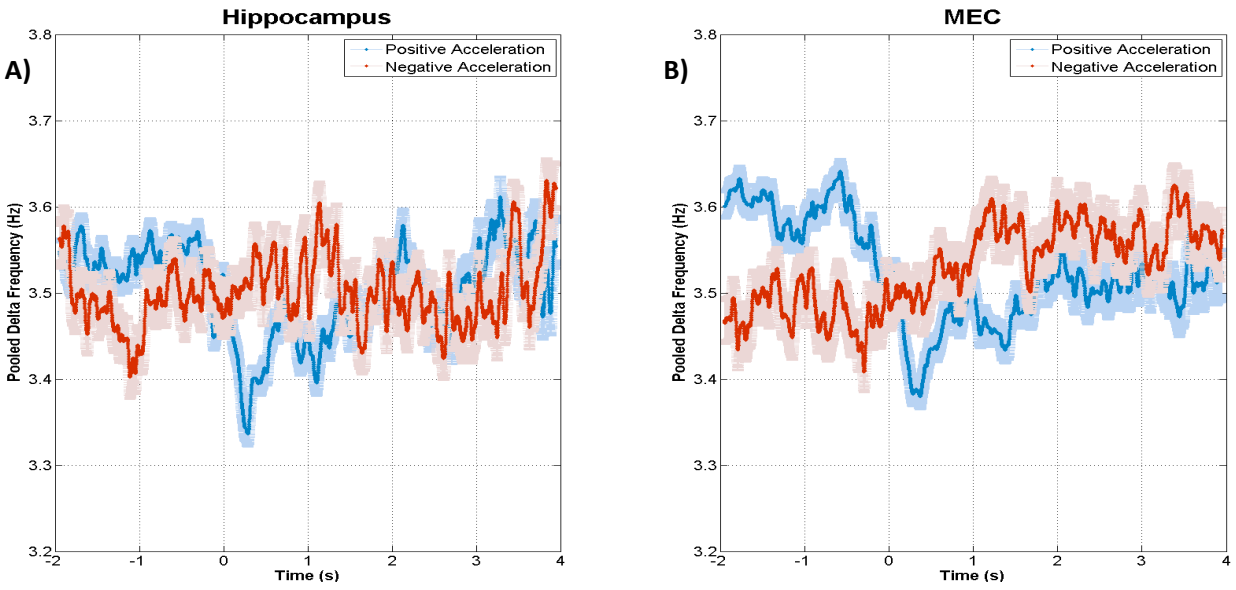

Figure 23: Delta frequency during acceleration (medians ±SEM). Unlike the theta band frequency, the delta signal shows a decrease during transitions from low speeds to higher ones. This was not found to follow any trend in the significant differences between the peak and baseline medians in either the hippocampus (**A**) or the MEC (**B**). **B**) The MEC seems to follow the tendency seen in the previous chapter for the delta frequency to decrease when the animal is engaged in movement at higher speeds and vice versa.

TABLE 4: Difference in Delta Frequency (Median Peak – Baseline in Hz)

Hippocampus

Prior Velocity \ New Velocity	8 cm/s	16 cm/s	24 cm/s	32 cm/s
8 cm/s	0	-0.06	-0.1	-0.13**
16 cm/s	0.14	0	0.17	0.04
24 cm/s	-0.1	-0.1	0	-0.31**
32 cm/s	0.22	0.19**	0.06	0

(P<0.05), **(P<0.01), *(P<0.001)*

MEC

Prior Velocity \ New Velocity	8 cm/s	16 cm/s	24 cm/s	32 cm/s
8 cm/s	0	-0.12**	-0.09**	-0.22***
16 cm/s	0.01	0	-0.13	-0.13
24 cm/s	0	-0.03	0	-0.07*
32 cm/s	0.15	0.11**	0.03	0

(P<0.05), **(P<0.01), *(P<0.001)*

Unlike the acceleration induced peak in theta frequency, the delta frequency failed to show any effect of the magnitude of the transitions to higher speeds in either of the drives following the Kruskal-Wallis test of variance (Hippocampus: H=0.41, 2 *d.f.,* P=0.81, MEC: H=1.35, 2 *d.f.,* P=0.51). A significant difference was not seen in the negative accelerations in the hippocampus or MEC (H=2.40, 2 *d.f.,* P=0.30, and H=2.37, 2 *d.f.,* P=0.31 respectively).

There was a strong effect of the prior speed on the degree of the peak following a transition with the slower initial speed evoking a greater effect. The value of the initial speed lead to significant differences in the delta frequency peaks for the three 8cm/s^2 accelerations (Hippocampus: H=23.88, 2 *d.f.,* P=6.53x10^{-6}, and MEC: H=53.17, 2 *d.f.,* P=6.26x10^{-8}). The Bonferroni test found the 8cm/s to 16cm/s and 24cm/s to 32cm/s conditions to be different (confirmed using the Wilcoxon rank sum H=4.94, 2 *d.f.,* P=7.91x10^{-7}). This difference was also present in the MEC except that all the 8cm/s^2 accelerations produced a difference in the peak values as a result of the different starting speeds (Wilcoxon: H=3.95, 2 *d.f.,* P=7.93x10^{-5}, H=5.38, 2 *d.f.,* P=7.65x10^{-8}) (Figure 24). The initial speed also had an effect on the magnitude of the peak seen in the 16cm/s^2 accelerations (hippocampus: H=4.86, 2 *d.f.,* P=1.20x10^{-6}, MEC: H=5.20, 2 *d.f.,* P=2.03x10^{-8}). The value of the prior speed had no effect on the delta frequency during transitions to the lower speeds in either recording site.

Together these findings serve to support the relationship seen between speed and the delta band frequency in the earlier section. The higher values are seen during periods or transitions to lower speeds while higher speeds have yielded a lower delta frequency in both drives. The lack of a regular pattern in the acceleration induced response suggests that the delta band is reacting differently to changes in speed than the theta band. This difference supports the notion that what is happening in the theta band is unique and not an EEG wide frequency phenomenon.

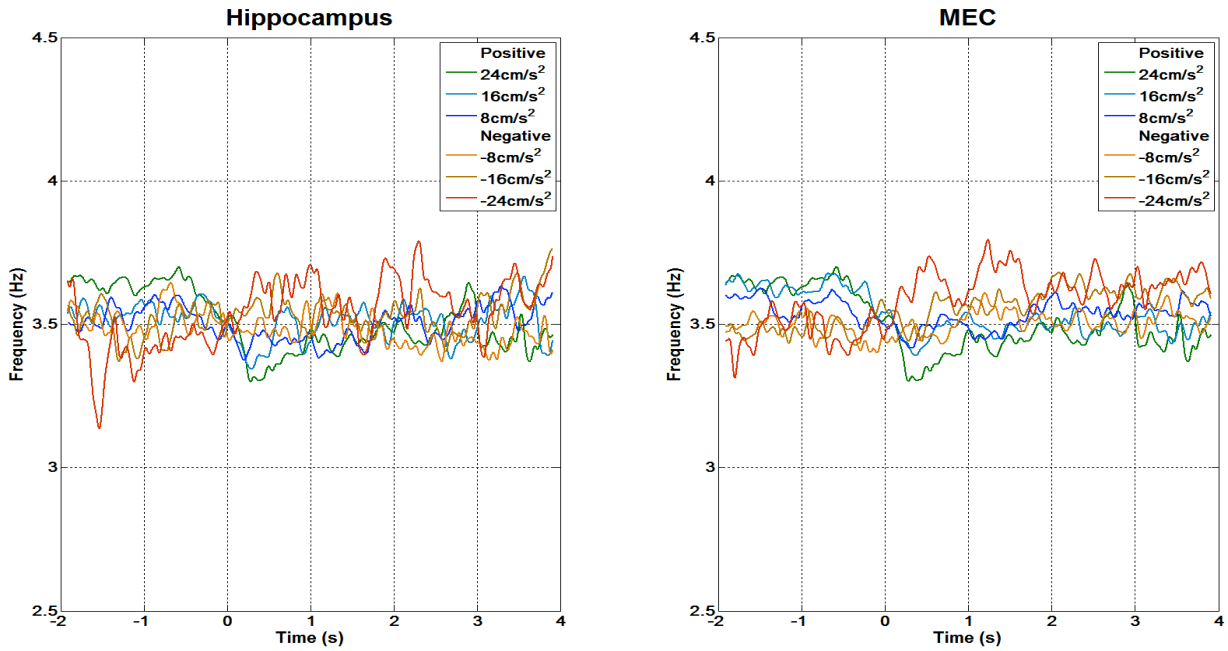

Figure 24: The effect of the magnitude of acceleration on the delta frequency. The differences between the peak values and the baseline in the positive and negative accelerations can be seen in both the hippocampus and MEC. Though the positive accelerations do seem so create a larger trough with larger changes in speed, the effect is not significant.

Amplitudes during Acceleration

The amplitude of the moments of acceleration were extracted in the same manner as the frequency values, however, as mentioned earlier the values suffered from trial by trial and electrode by electrode variability and thus needed to be normalized Therefore all the amplitude values seen here are expression of the percentage of the 8cm/s baseline. This normalization allowed for the same statistical test to be applied as those in the frequency analysis. The amplitude values for both the theta and delta bands showed a similar response to the transitions in speed and the analysis of the amplitudes in both bands have been combined in this section for convenience.

Both the delta and theta band amplitudes showed the same acceleration induced peak during positive acceleration although the theta band produced a much greater peak (Figure 25). The differences lie in the manner in which the negative acceleration affected the amplitude. Though the analysis of the effect of constant running speed on the hippocampal theta amplitude did not yield a significant difference, there was a slight increase in the amplitude as speed increased which could explain the difference in the amplitude prior to the transition in the negative accelerations. The effect of increasing the speed on the theta amplitude in the MEC had been established in the previous section. Since all the negative accelerations begin with values greater than 8cm/s (the normalizing value), it is expected that the MEC would have higher amplitude prior to transition in those cases. The trough seen at the time of transition in the

hippocampal theta amplitude is unique amongst the acceleration-induced responses compared to the delta amplitude and theta frequency. The effect of speed on the amplitude of the delta signal has been shown in the previous section to only have a significant effect of decreasing the amplitude with increasing speed in the MEC. This is consistent with the values seen in Figure 25 (C,D). The results from the analysis of the theta and delta amplitude are summarized in Table 5.

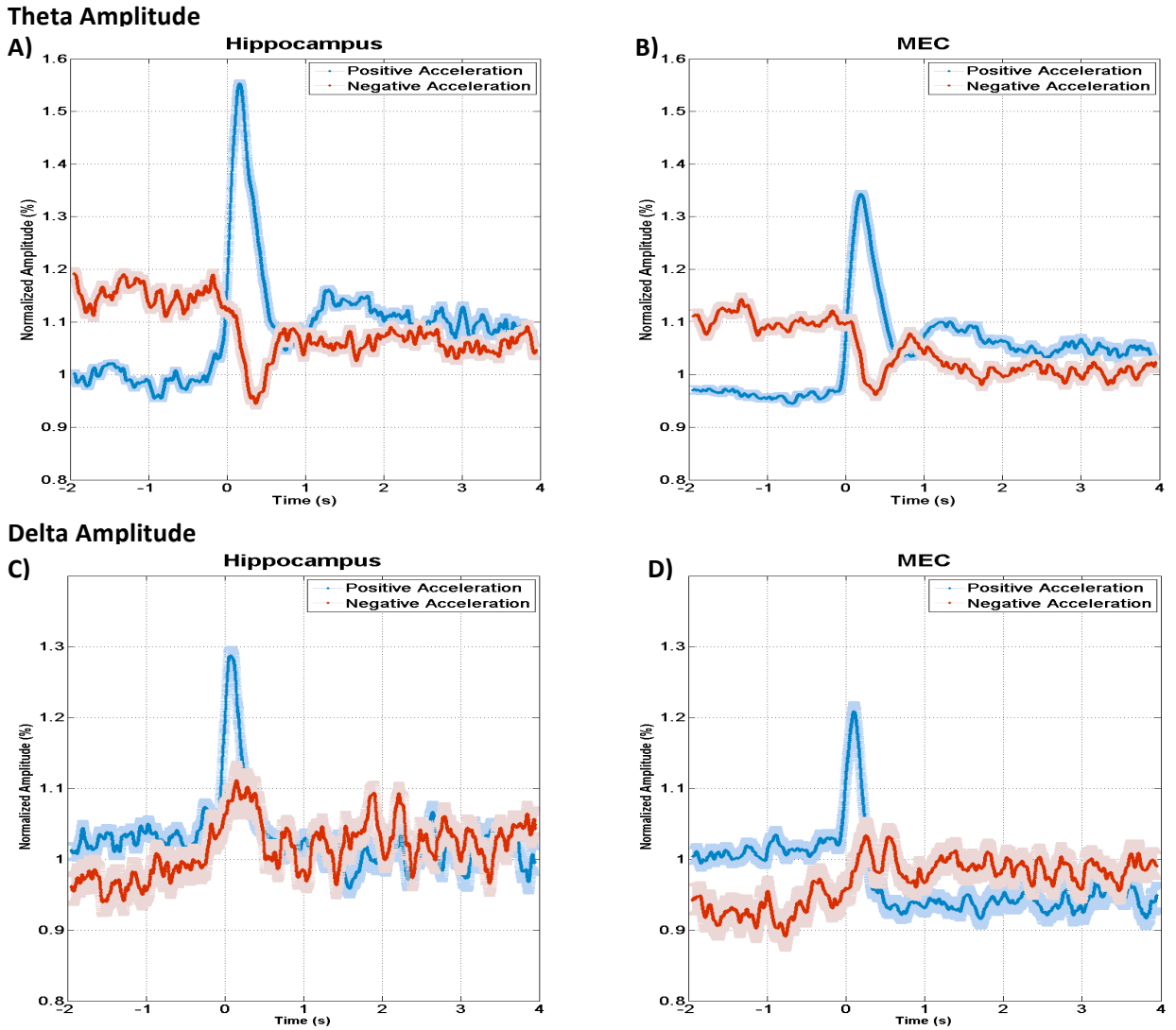

Figure 25: Pooled median amplitudes of all positive (blue) and negative (red) accelerations in both the theta and delta bands in the hippocampus and MEC (±SEM). **A**) There is a clear difference between the low and high speeds prior to the transition. Unlike the nearly unchanging theta frequency in response to negative acceleration, instead both the hippocampal and medial entorhinal theta amplitude show trough **B**) The MEC theta amplitude has been shown in the previous section to increase with increasing speed this case exemplifies this effect, with the addition of an acceleration effect. Notice the smaller peak value compared to the one achieved in the hippocampus. **C/D**) The delta amplitudes of the hippocampus and MEC follow the same trend in the positive accelerations as the theta amplitude and frequency. However, the amplitude shows speed modulation the MEC, seen here as a rise in amplitude as a result of a transition to a lower speed and vice versa for the positive acceleration.

TABLE 6: Summary of the Acceleration Analysis for the Theta and Delta Band Amplitudes

Theta Amplitude

Hippocampus		New Speed 8 cm/s	16 cm/s	24 cm/s	32 cm/s	MEC		New Speed 8 cm/s	16 cm/s	24 cm/s	32 cm/s
Prior Speed	8 cm/s	0	0.35***	0.51***	0.67***	Prior Speed	8 cm/s	0	0.24***	0.36***	0.47***
	16 cm/s	-0.15	0	-0.06	0.36***		16 cm/s	-0.04	0	0.21***	0.29***
	24 cm/s	-0.07	0.02	0	0.39***		24 cm/s	0.05	0.12*	0	0.26***
	32 cm/s	0	-0.18**	-0.05	0		32 cm/s	-0.12**	-0.08**	-0.05	0

*(P<0.05), **(P<0.01), ***(P<0.001)

Magnitude Effect

Positive Acceleration	H=93.55, 2df, *P*=4.85x10^21	Positive Acceleration	H=108.62, 2df, P=2.50x10^24
Negative Acceleration	H=9.07, 2df, P=0.01	Negative Acceleration	H=1.13, 2df, P=0.58

Delta Amplitude

Hippocampus		New Speed 8 cm/s	16 cm/s	24 cm/s	32 cm/s	MEC		New Speed 8 cm/s	16 cm/s	24 cm/s	32 cm/s
Prior Speed	8 cm/s	0	0.2***	0.33***	0.38***	Prior Speed	8 cm/s	0	0.04***	0.15***	0.27***
	16 cm/s	0.04	0	0.08	0.18		16 cm/s	0.08	0	0.07*	0.28***
	24 cm/s	0.25**	0.11*	0	0.24***		24 cm/s	0.12**	0.07*	0	0.14***
	32 cm/s	0.2***	0.12**	0.03	0		32 cm/s	0.17**	-0.02	0.01	0

*(P<0.05), **(P<0.01), ***(P<0.001)

Magnitude Effect

Positive Acceleration	H=29.28, 2df, *P*=4.38x10^7	Positive Acceleration	H=117.09, 2df, *P*=3.75x10^26
Negative Acceleration	H=6.31, 2df, *P*=0.04	Negative Acceleration	H=4.76, 2df, *P*=0.09

The quantification of the effects induced by acceleration on the theta frequency and amplitude and the delta amplitude in the hippocampus and MEC yielded a novel effect of acceleration on the LFP. The typical acceleration peak seen during a transition from a lower speed to a higher speed in combination with the results from the previous section on the effects of constant speeds, not only sheds doubt on the proposed and reported positive relationship between theta frequency and speed, but also adds another possible mechanism for encoding space in the brain.

Summary of the Results

The analysis of the stationary running speeds at four different velocities has failed to yield a modulatory effect on the theta band frequency in the medial entorhinal cortex and only a mild difference in the 8cm/s condition in the hippocampus. This later result was unexpected since the values reported in the literature show an increase in theta with increasing speed, thus predicting that, if anything, the 8cm/s condition should be lower than the other speeds. This lack of modulation in the MEC contradicts the current literature on the subject of theta rhythms and their relation to running speed. There was a modulatory effect on the delta frequency in both the MEC

and hippocampus. The amplitudes in both the bands displayed a progressive relationship with speed in the MEC, while only the delta amplitude was affected in the hippocampus.

A novel finding was also established in this section. Through the analysis of the constant running speeds we were unable to find a modulatory effect of speed on the theta frequency in the MEC. We also found that the acceleration of the animal does modulate the theta frequency in a profound manner that is scalable with the magnitude of the acceleration. This acceleration-induced peak in the frequency of the theta band was also seen in the amplitudes of both the theta and delta oscillations, but not observed in the delta frequency. This has some stark implications for the manner in which the theta frequency is treated in relation to self-movement in the hippocampus and MEC.

Discussion

The Experiment

There is a degree of inconsistency in the current literature regarding the relationship between the movement speed of an animal and the theta band (7-12Hz) frequency in the medial entorhinal cortex and hippocampal CA1 region. Previous reports had questionable evidence of a mild (McFarland et al., 1975; Rivas et al., 1996; Slawinska and Kasicki, 1998; Czurko et al., 1999; Maurer et al., 2005) to strong (Maurer et al., 2005; Jeewajee et al., 2008) speed/theta relationship. The lack of consistency in these findings is likely derived from the inability of previous studies to properly measure the theta rhythms of a moving animal without sacrificing their engagement in the movement by keeping them in a wheel or on a treadmill, and thus removing the sensation of motion. Other studies have suffered from the inaccuracy of sampling the LFP using small or broadly smoothed quanta of constant speeds in the freely moving animal. These later measures also failed to address non-constant movements such as turns and accelerations and have not attempted to dissociate the highly correlated acceleration and speed variables while the rat moves (for a visual representation of the correlation between speed and acceleration in the open field see appendix C). Since these two elements are so closely correlated it is very likely that when an experiment claims to be measuring running speed, they are actually taking in moments of acceleration.

The most recent and most influential of these studies reporting a relationship between theta frequency and running speed has been the linear relationship in the MEC of rats described by Jeewajee et al. (2008). Several models have been developed to describe the phenomenon seen in the spatial navigation and path integration system in the brain and have drawn support from Jeewajee et al.'s dogmatic near linear relationship. The first goal of the experiment was to address the findings of the Jeewajee et al. experiment (as well as others) and its implications in the dual oscillatory model of theta phase precession in place cells (O'Keefe and Recce, 1993) and grid cells and the Burgess (2008) multiple oscillatory model for grid cell formation based on an expansion of the one dimensional dual oscillatory model into two dimensions. The key element in these models is the coding of distance travelled following a linear relationship between running speed and theta or theta-like oscillations. To determine the validity of the previous publications related to the relationship between self-movement speed and the theta band frequency and by extension the models that assume this linear relationship exists, a novel protocol was developed to better record and analyze the movements of an animal at a specific constant speed and to assess the effects of any sudden changes to these speeds. The advantage of this new apparatus was its ability to dissociate the effects of acceleration from the effects of constant speed, which as mentioned before, is integral to properly understanding this speed/theta relationship.

Main Findings: Speed and Theta

Since speed is the derivative of position in time, and frequency is the derivative of the phase of an oscillation, then it can be extrapolated that if these two values are directly proportional, then the phase of an oscillation would be related to the position of an animal. Since this relationship has been claimed to be the case for running speed and theta oscillations (which according to our results is not the case), O'Keefe and Recce (1993) and Burgess (2008) have assumed that the running speed of an animal will encode changes in position via the frequency of the theta oscillation, as the phase would vary directly with the speed with which the animal traverses the environment. These dual oscillator models use this speed/theta relationship to determine the movement of an animal through a location using the animals speed to determine its position relative to the field of a place cell and thus can create phase precession. Should the linear relationship between speed and theta frequency turn out to not be directly proportional in the MEC, then the oscillator interference model in its current state cannot explain both grid maps and phase precession. Through the results of this project and the ability of the apparatus to dissociate between speed and acceleration, we have been able to show that this linear relationship does not exist on the grounds that speed does not modulate theta frequency in the MEC.

This finding also upsets the expanded 2 dimensional versions of the dual oscillator model to a multiple oscillatory model (Burgess, 2008; Jeewajee et al., 2008) which attempts to explain grid cell firing based on the directional input of velocity sensitive theta oscillations with a linear speed/frequency relationship, that when they are in phase they will elicit a response in a coincidence detector (grid cell) and lead to the characteristic firing pattern of grid cells in MEC. Without this directly proportional speed modulated theta frequency relationship, these models cannot determine the location of the rat without adding in compensating variables. Jeewajee et al. (2008) had claimed to have found this linear relationship in the MEC of freely behaving rats. However, using a stricter paradigm for controlling the speed of the rat and isolating variables such as instantaneous acceleration, we have found that is to not the case in the MEC, and with the exception of the lowest speed, not the case in the hippocampus either.

By assuming that the recordings made in the open field sessions were only the result of constant velocity based on the instantaneous measurements taken, Jeewajee et al. (2008) might have failed to dissociate speed from acceleration thus making an incorrect claim about speed modulation when in fact this could be entirely based on the acceleration induced changes in the theta frequency in the MEC and hippocampus, discussed in detail in the following subsection.

Main Findings: Acceleration and Theta

The second major finding in this study was the existence of a positive acceleration based modulation of the theta frequency in the hippocampal and medial entorhinal cortices. This modulation came in the form of a sudden and sharp increase in the theta frequency during transitions from lower speeds to higher ones. The 'acceleration induced peak' was observed to

produce a peak of up to 0.36Hz above baseline in the hippocampus and up to 0.46Hz above baseline in the MEC. The peak would typically last up to 500ms following the onset, a typical time that is consistent with the time that it took for rats to accelerate in pilot studies. This effect was also seen to increase with the magnitude of the acceleration so that greater accelerations would produce greater peak values following a transition. Transitions from a higher speed to a lower one failed to produce a significant difference in the theta frequency with the exception of the -16cm/s^2 acceleration in the hippocampus but not in the MEC, suggesting that positive acceleration is the only movement related variable to alter the theta frequency.

The results from the Jeewajee et al. (2008) study need not be considered totally incorrect, but instead they are possibly a misnomer of attributing acceleration induced changes in the theta frequency to being caused by running speed. As we have seen in this experiment, the positive acceleration of the animal is having a profound effect on the theta frequency leading to sudden and substantial peaks following a transition to a higher speed. Jeewajee and colleagues claim to have sampled the movements of the rats in the open field at 50Hz and then smoothed the data over 500ms. This smoothing could flatten the 500ms acceleration induced peaks seen in the data from this study. Since the acceleration induced peaks seen in the theta frequency take place within 500ms following a transition and only during positive accelerations, it is entirely possible that the measures of increased frequency with speed were in fact only the positive values in the peak smoothed to render only an increase in the frequency attributed to the higher speed. We have shown here that there is a strong effect of the magnitude of the positive acceleration on the intensity of the increase in the theta frequency. It is possible that since the Jeewajee et al. study was smoothing recording epochs that the acceleration modulation was incorrectly being associated with a speed signal. In short, the observation of a correlation between speed and theta frequency by Jeewajee and colleagues could be quasi correct, since theta frequency is driven by positive acceleration and speed and acceleration are two variables that are tightly related (one being the derivative of the other).

Additional Finding: Other Measures of Speed and Acceleration Modulation

We were able to show a significant decrease in the delta frequency during progressively faster running speeds, suggesting a negative relationship. However, acceleration failed to elicit a consistently significant response in the delta band frequency. Due to the limited understanding of the biophysical mechanisms of the delta oscillation it becomes difficult to make any conclusions based on the limited literature. One interesting finding from the lack of an acceleration response in the delta band is that this confirms that the theta acceleration induced peak is a band specific response rather than an identical change across multiple EEG bands.

This study also found that there was a difference in the delta and theta amplitude based on the speed of the animal and the acceleration. The theta amplitude seemed to increase with faster speeds, while the delta amplitude seemed to decrease, suggesting different forms of speed

modulation exist in either band. However both the theta and delta amplitudes produced the same positive acceleration peak as seen in the theta frequency. The only difference being that in the theta amplitude there was a trough produced in the amplitude during negative accelerations. These changes in the amplitude again suggest that a different mechanism may be at work in the modulation of the amplitudes, however positive acceleration seems to have a consistent effect which could be indicative of a factor that is shared across both bands.

Possible Limitation on the Hippocampal Data

The claim that theta frequency in the hippocampus is modulated only by positive acceleration is challenged by the appearance of a positive peak in the frequency while all the other negative accelerations did not produce any effect. We have found that there was a negative relationship between the running speeds of the animal and the occurrence of head movements. These head movements have been shown to affect the theta frequency and thus could explain the increased variance in the theta frequency at lower speeds. This is an understandable phenomenon since the animal is less engaged in the movements at lower speeds and is thus paying less attention to the cart thereby leaving more time for exploration. The more likely cause of this unexpected response to negative acceleration could also be due to the lower number of samples in these two speeds due to occasional poor EEG recordings in the hippocampal drives alone. In response to the quality issue, the data was put through a filter that would identify and remove poor EEG recordings thereby reducing the number of usable trials. When the control over the quality of the recordings is more lax, this trend seems to be alleviated, suggesting that this is only a matter of statistical power not an actual trend.

Future Considerations

The results of this experiment are contradictory to the conclusion reached by Jeewajee et al. (2008), however their experiment used an open field analysis, which as explained earlier makes the dissociation between acceleration and speed very difficult. To determine if the cart itself was leading to any changes in the behaviour or oscillations of the animal it is desirable to devise a new method for recoding a free rat in the open field.

A second test to determine if there is any effect of predictability on the changes in the theta and delta band oscillations would provide insight in the acceleration based modulation of the theta frequency, as well as determining if knowledge of a transition in speed will alter the amplitudes of the delta and theta oscillations based on expectation. Based on the findings reported by Lisman et al., (2010) it has been shown that the delta oscillation is related to dopaminergic control, a neurotransmitter associated with reward. It has previously been shown by Ungless et al. (2002) that the dopaminergic neurons of the ventral tegmental area (VT) are inhibited by aversive stimuli. Since the hippocampus plays a direct role in the release of dopamine in the VTA, it is possible that the thalamo-hippocampo-ventral tegmental loop is in fact encoding an aversive state when the animal is engaged in higher speed movement. Since the

8cm/s condition seems to have little effect on the hippocampal it could be assumed that this is the normal state of the rat and any perturbation of this state will be signalled by a decrease in the hippocampal delta frequency which in turn will lead to deceased dopamine release in the ventral tegmental area (Lisman et al., 2010). Based on the current analysis any conclusions related to this topic are not possible. The design of the experiment does offer a manner to test for any predictability signals. Since each lap contained a constant and variable transition point between the speed regions in each direction of the lap (inbound and outbound) an analysis could be made of the differences in the delta and theta oscillations as a result of a learning to associate a place with an acceleration. Should any differences appear, this would suggest that some form of memory based modulation (possibly reward based in the delta band according to Lisman et al. 2010) of the acceleration response is present.

A major question that arises out of this study is related to the source of mechanism by which these moments of acceleration are detected and how they are able to alter the state of the theta frequency and amplitude, as well as the delta amplitude across large areas of the hippocampus and MEC. It is possible to remove factors that would influence the perception of motion such as optic flow, vestibular input, and sensory feedback from muscular engagement in locomotion, as had been done by Terrazas et al. (2005), but these results were not as conclusive as expected since the theta frequency and firing pattern of neurons were still effected by motion but to a lesser degree. We expect that the effect of acceleration on theta frequency, for example, will still be present but somehow smeared out by the partial absence of cues.

Conclusion

By strictly controlling the movement speed of a rat that is freely engaging in locomotion, we have been able to discern between speed and acceleration based modulation of the theta and delta band oscillations in the hippocampus and medial entorhinal cortex. We have found that there is no effect of running speed on the frequency of the theta oscillation in the medial entorhinal cortex, a result that questions the linear relationship reported in the literature. This also leads to implications in the validity of modeling certain phenomena in the hippocampus and medial entorhinal cortex based on this assumed linear relationship between movement speed and the theta frequency. If path integration is being computed in this region of the brain, the velocity signal has to come coded in a different way, such as the firing of neurons for example. The second major result of this experiment was that rather than the speed of the animal leading to modulation of the theta signal, instead it was discovered that positive acceleration was the only factor that altered MEC theta frequency. Since speed and acceleration are so highly correlated, it is possible that past measures of speed induced changes to the theta frequency in the hippocampus and MEC have been erroneously attributed to speed and not acceleration. Future research into the modulation of hippocampal and medial entorhinal oscillations and cell types during moments of acceleration could help to decipher the mechanisms by which the brain encodes movement through space.

References

1. Alonso, A. & Garciaaustt, E. Neuronal sources of theta rhythm in the entorhinal cortex of the rat .1. Laminar distribution of theta field potentials. *Experimental Brain Research* **67**, 493-501 (1987).

2. Alonso, A. & Garciaaustt, E. Neuronal sources of theta rhythm in the entorhinal cortex of the rat .2. Phase-relations between unit discharges and theta field potentials. *Experimental Brain Research* **67**, 502-509 (1987).

3. Amaral, D.G. & Witter, M.P. the 3-dimensional organization of the hippocampal-formation - a review of anatomical data. *Neuroscience* **31**, 571-591 (1989).

4. Andersen, P., Bliss, T.V.P. & Skrede, K.K. lamellar organization of hippocampal excitatory pathways. *Experimental Brain Research* **13**, 222-& (1971).

5. Andersen, P., Morris, R.G., Amaral, D.G., Bliss, T. & O'Keefe, J. *The Hippocampus Book* (Oxford University Press, New York, 2007).

6. Anderson, M.I. & Jeffery, K.J. Heterogeneous modulation of place cell firing by changes in context. *Journal of Neuroscience* **23**, 8827-8835 (2003).

7. Blair, H.T., Welday, A.C. & Zhang, K.C. Scale-invariant memory representations emerge from moire interference between grid fields that produce theta oscillations: A computational model. *Journal of Neuroscience* **27**, 3211-3229 (2007).

8. Bland, B.H., Colom, L.V., Konopacki, J. & Roth, S.H. intracellular records of carbachol-induced theta-rhythm in hippocampal slices. *Brain Research* **447**, 364-368 (1988).

9. Bland, B.H., Colom, L.V. & Oddie, S.D. dorsomedial-posterior hypothalamic influences on the septo-hippocampal pathway in the generation of hippocampal theta. *Society for Neuroscience Abstracts* **17**, 1036 (1991).

10. Bland, B.H. & Whishaw, I.Q. generators and topography of hippocampal theta (rsa) in anesthetized and freely moving rat. *Brain Research* **118**, 259-280 (1976).

11. Bostock, E., Muller, R.U. & Kubie, J.L. Experience-dependent modifications of hippocampal place cell firing. *Hippocampus* **1**, 193-205 (1991).

12. Brun, V.H., *et al.* Place cells and place recognition maintained by direct entorhinal-hippocampal circuitry. *Science* **296**, 2243-2246 (2002).

13. Burgess, N. Grid Cells and Theta as Oscillatory Interference: Theory and Predictions. *Hippocampus* **18**, 1157-1174 (2008).

14. Burgess, N., Barry, C. & O'Keefe, J. An oscillatory interference model of grid cell firing. *Hippocampus* **17**, 801-812 (2007).

15. Burgess, N. & O'Keefe, J. Models of place and grid cell firing and theta rhythmicity. *Current Opinion in Neurobiology* **21**, 734-744 (2011).

16. Buzsaki, G. *Rhythms of the Brain* (Oxford University Press, New York, 2006).

17. Buzsaki, G. The thalamic clock - emergent network properties. *Neuroscience* **41**, 351-364 (1991).

18. Buzsaki, G. Theta oscillations in the hippocampus. *Neuron* **33**, 325-340 (2002).

19. Buzsaki, G., Freund, T.F., Bayardo, F. & Somogyi, P. Ischemia-induced changes in the electrical-activity of the hippocampus. *Experimental Brain Research* **78**, 268-278 (1989).

20. Chrobak, J.J., Lorincz, A. & Buzsaki, G. Physiological patterns in the hippocampo-entorhinal cortex system. *Hippocampus* **10**, 457-465 (2000).

21. Csicsvari, J., Jamieson, B., Wise, K.D. & Buzsaki, G. Mechanisms of gamma oscillations in the hippocampus of the behaving rat. *Neuron* **37**, 311-322 (2003).

22. Czurko, A., Hirase, H., Csicsvari, J. & Buzsaki, G. Sustained activation of hippocampal pyramidal cells by 'space clamping' in a running wheel. *European Journal of Neuroscience* **11**, 344-352 (1999).

23. Deshmukh, S.S., Yoganarasimha, D., Voicu, H. & Knierim, J.J. Theta Modulation in the Medial and the Lateral Entorhinal Cortices. *Journal of Neurophysiology* **104**, 994-1006 (2010).

24. Dhillon, A. & Jones, R.S.G. Laminar differences in recurrent excitatory transmission in the rat entorhinal cortex in vitro. *Neuroscience* **99**, 413-422 (2000).

25. Douglas, R.J. Hippocampus and behavior. *Psychological Bulletin* **67**, 416-& (1967).

26. Efron, B. Nonparametric estimates of standard error - the jackknife, the bootstrap and other methods. *Biometrika* **68**, 589-599 (1981).

27. Eichenbaum, H., Dudchenko, P., Wood, E., Shapiro, M. & Tanila, H. The hippocampus, memory, and place cells: Is it spatial memory or a memory space? *Neuron* **23**, 209-226 (1999).

28. Freund, T.F. & Buzsaki, G. Interneurons of the hippocampus. *Hippocampus* **6**, 347-470 (1996).

29. Fujisawa, S. & Buzsaki, G. A novel (4 Hz) oscillation of prefrontal and hippocampal neurons in the waking rat. *Society for Neuroscience Abstract Viewer and Itinerary Planner* **39** (2009).

30. Fujisawa, S. & Buzsaki, G. A 4 Hz Oscillation Adaptively Synchronizes Prefrontal, VTA, and Hippocampal Activities. *Neuron* **72**, 153-165 (2011).

31. Fyhn, M., Molden, S., Witter, M.P., Moser, E.I. & Moser, M.B. Spatial representation in the entorhinal cortex. *Science* **305**, 1258-1264 (2004).

32. Geisler, C., Robbe, D., Zugaro, M., Sirota, A. & Buzsaki, G. Hippocampal place cell assemblies are speed-controlled oscillators. *Proceedings of the National Academy of Sciences of the United States of America* **104**, 8149-8154 (2007).

33. Giocomo, L.M. & Hasselmo, M.E. Knock-Out of HCN1 Subunit Flattens Dorsal-Ventral Frequency Gradient of Medial Entorhinal Neurons in Adult Mice. *Journal of Neuroscience* **29**, 7625-7630 (2009).

34. Giocomo, L.M.*, et al.* Grid Cells Use HCN1 Channels for Spatial Scaling. *Cell* **147**, 1159-1170 (2011).

35. Giocomo, L.M., Zilli, E.A., Fransen, E. & Hasselmo, M.E. Temporal frequency of subthreshold oscillations scales with entorhinal grid cell field spacing. *Science* **315**, 1719-1722 (2007).

36. Gray, C.M., Maldonado, P.E., Wilson, M. & McNaughton, B. Tetrodes markedly improve the reliability and yield of multiple single-unit isolation from multi-unit recordings in cat striate cortex. *Journal of Neuroscience Methods* **63**, 43-54 (1995).

37. Green, J.D. & Arduini, A.A. HIPPOCAMPAL ELECTRICAL ACTIVITY IN AROUSAL. *Journal of Neurophysiology* **17**, 533-557 (1954).

38. Hafting, T., Fyhn, M., Molden, S., Moser, M.B. & Moser, E.I. Microstructure of a spatial map in the entorhinal cortex. *Nature* **436**, 801-806 (2005).

39. Hafting, T., Fyhn, M., Bonnevie, T., Moser, M.-B. & Moser, E.I. Hippocampus-independent phase precession in entorhinal grid cells. *Nature* **453**, 1248-U1250 (2008).

40. Harper, R.M. frequency changes in hippocampal electrical activity during movement and tonic immobility. *Physiology & Behavior* **7**, 55-& (1971).

41. Hasselmo, M.E. & Fehlau, B.P. Differences in time course of ACh and GABA modulation of excitatory synaptic potentials in slices of rat hippocampus. *Journal of Neurophysiology* **86**, 1792-1802 (2001).

42. Hasselmo, M.E. & Brandon, M.P. Linking Cellular Mechanisms to Behavior: Entorhinal Persistent Spiking and Membrane Potential Oscillations May Underlie Path Integration, Grid Cell Firing, and Episodic Memory. *Neural Plasticity*, 658323 (2008).

43. Jeewajee, A., Barry, C., O'Keefe, J. & Burgess, N. Grid Cells and Theta as Oscillatory Interference: Electrophysiological Data From Freely Moving Rats. *Hippocampus* **18**, 1175-1185 (2008).

44. Jeffery, K.J. & Anderson, M.I. Dissociation of the geometric and contextual influences on place cells. *Hippocampus* **13**, 868-872 (2003).

45. Jouvet, M. Biogenic amines and states of sleep. *Science* **163**, 32-& (1969).

46. Kentros, C.*, et al.* Abolition of long-term stability of new hippocampal place cell maps by NMDA receptor blockade. *Science* **280**, 2121-2126 (1998).

47. King, C., Recce, M. & O'Keefe, J. The rhythmicity of cells of the medial septum diagonal band of Broca in the awake freely moving rat: relationships with behaviour and hippocampal theta. *European Journal of Neuroscience* **10**, 464-477 (1998).

48. Kjelstrup, K.B., *et al.* Finite scale of spatial representation in the hippocampus. *Science* **321**, 140-143 (2008).

49. Kohler, C. A projection from the deep layers of the entorhinal area to the hippocampal-formation in the rat-brain. *Neuroscience Letters* **56**, 13-19 (1985).

50. Kramis, R., Vanderwolf, C.H. & Bland, B.H. 2 types of hippocampal rhythmical slow activity in both rabbit and rat - relations to behavior and effects of atropine, diethyl-ether, urethane, and pentobarbital. *Experimental Neurology* **49**, 58-85 (1975).

51. Lakatos, P., Karmos, G., Mehta, A.D., Ulbert, I. & Schroeder, C.E. Entrainment of neuronal oscillations as a mechanism of attentional selection. *Science* **320**, 110-113 (2008).

52. Lee, M.G., Chrobak, J.J., Sik, A., Wiley, R.G. & Buzsaki, G. Hippocampal theta-activity following selective lesion of the septal cholinergic system. *Neuroscience* **62**, 1033-1047 (1994).

53. Leung, L.S., Roth, L. & Canning, K.J. entorhinal inputs to hippocampal ca1 and dentate gyrus in the rat - a current-source-density study. *Journal of Neurophysiology* **73**, 2392-2403 (1995).

54. Leung, L.W.S. model of gradual phase-shift of theta-rhythm in the rat. *Journal of Neurophysiology* **52**, 1051-1065 (1984).

55. Leung, L.W.S. & Yim, C.Y. intracellular records of theta rhythm in hippocampal ca1 cells of the rat. *Brain Research* **367**, 323-327 (1986).

56. Lilliefo.Hw. On kolmogorov-smirnov test for normality with mean and variance unknown. *Journal of the American Statistical Association* **62**, 399-& (1967).

57. Lisman, J.E., Pi, H.J., Zhang, Y.C. & Otmakhova, N.A. A Thalamo-Hippocampal-Ventral Tegmental Area Loop May Produce the Positive Feedback that Underlies the Psychotic Break in Schizophrenia. *Biological Psychiatry* **68**, 17-24 (2010).

58. Maurer, A.P., VanRhoads, S.R., Sutherland, G.R., Lipa, P. & McNaughton, B.L. Self-motion and the origin of differential spatial scaling along the septo-temporal axis of the hippocampus. *Hippocampus* **15**, 841-852 (2005).

59. McFarland, W.L., Teitelbaum, H. & Hedges, E.K. relationship between hippocampal theta activity and running speed in rat. *Journal of Comparative and Physiological Psychology* **88**, 324-328 (1975).

60. McNaughton, B.L., Battaglia, F.P., Jensen, O., Moser, E.I. & Moser, M.-B. Path integration and the neural basis of the 'cognitive map'. *Nature Reviews Neuroscience* **7**, 663-678 (2006).

61. Mitchell, S.J. & Ranck, J.B. generation of theta rhythm in medial entorhinal cortex of freely moving rats. *Brain Research* **189**, 49-66 (1980).

62. Miyasaka, M. & Domino, E.F. neuronal mechanisms of ketamine-induced anesthesia. *International Journal of Neuropharmacology* **7**, 557-& (1968).

63. Mizuseki, K., Sirota, A., Pastalkova, E. & Buzsaki, G. Theta Oscillations Provide Temporal Windows for Local Circuit Computation in the Entorhinal-Hippocampal Loop. *Neuron* **64**, 267-280 (2009).

64. Moser, E.I., Kropff, E. & Moser, M.-B. Place cells, grid cells, and the brain's spatial representation system. *Annual Review of Neuroscience* **31**, 69-89 (2008).

65. Muller, R.U. & Kubie, J.L. the effects of changes in the environment on the spatial firing of hippocampal complex-spike cells. *Journal of Neuroscience* **7**, 1951-1968 (1987).

66. Naber, P.A., da Silva, F.H.L. & Witter, M.P. Reciprocal connections between the entorhinal cortex and hippocampal fields CA1 and the subiculum are in register with the projections from CA1 to the subiculum. *Hippocampus* **11**, 99-104 (2001).

67. Navratilova, Z., Giocomo, L.M., Fellous, J.M., Hasselmo, M.E. & McNaughton, B.L. Phase precession and variable spatial scaling in a periodic attractor map model of medial entorhinal grid cells with realistic after-spike dynamics. *Hippocampus* **22**, 772-789 (2012).

68. Norman, G. & Eacott, M.J. Dissociable effects of lesions to the perirhinal cortex and the postrhinal cortex on memory for context and objects in rats. *Behavioral Neuroscience* **119**, 557-566 (2005).

69. O'Keefe, J. & Nadel, L. *The Hippocampus as a Cognitive Map* (Clarendon Press, Oxford, 1978).

70. Okeefe, J. & Dostrovs.J. Hippocampus as a spatial map - preliminary evidence from unit activity in freely-moving rat. *Brain Research* **34**, 171-& (1971).

71. Okeefe, J. & Recce, M.L. phase relationship between hippocampal place units and the eeg theta-rhythm. *Hippocampus* **3**, 317-330 (1993).

72. Paxinos, G. & Watson, C. *The Rat Brain in Stereotaxic Coordinates* (Elsevier, London, 2007).

73. Petsche, H., Gogolak, G. & Stumpf, C. Significance of rabbits septum as a relay station between midbrain and hippocampus .1. Control of hippocampus arousal activity by septum cells. *Electroencephalography and Clinical Neurophysiology* **14**, 202-& (1962).

74. Quilichini, P., Sirota, A. & Buzsaki, G. Intrinsic Circuit Organization and Theta-Gamma Oscillation Dynamics in the Entorhinal Cortex of the Rat. *Journal of Neuroscience* **30**, 11128-11142 (2010).

75. Rivas, J., Gaztelu, J.M. & GarciaAustt, E. Changes in hippocampal cell discharge patterns and theta rhythm spectral properties as a function of walking velocity in the guinea pig. *Experimental Brain Research* **108**, 113-118 (1996).

76. Romani, S., Sejnowski, T.J. & Tsodyks, M. Intracellular Dynamics of Virtual Place Cells. *Neural Computation* **23**, 651-655 (2011).

77. Sainsbury, R.S., Heynen, A. & Montoya, C.P. behavioral-correlates of hippocampal type-2 theta in the rat. *Physiology & Behavior* **39**, 513-519 (1987).

78. Sargolini, F.*, et al.* Conjunctive representation of position, direction, and velocity in entorhinal cortex. *Science* **312**, 758-762 (2006).

79. Shin, J. & Talnov, A. A single trial analysis of hippocampal theta frequency during nonsteady wheel running in rats. *Brain Research* **897**, 217-221 (2001).

80. Slawinska, U. & Kasicki, S. The frequency of rat's hippocampal theta rhythm is related to the speed of locomotion. *Brain Research* **796**, 327-331 (1998).

81. Solstad, T., Boccara, C.N., Kropff, E., Moser, M.-B. & Moser, E.I. Representation of Geometric Borders in the Entorhinal Cortex. *Science* **322**, 1865-1868 (2008).

82. Sprent, P. & Smeeton, N.C. *Applied Nonparametric staistical Methods* (Chapman and Hall/CRC, New York, 2000).

83. Tamamaki, N. & Nojyo, Y. Preservation of topography in the connections between the subiculum, field ca1, and the entorhinal cortex in rats. *Journal of Comparative Neurology* **353**, 379-390 (1995).

84. Taube, J.S. head direction cells recorded in the anterior thalamic nuclei of freely moving rats. *Journal of Neuroscience* **15**, 70-86 (1995).

85. Taube, J.S., Muller, R.U. & Ranck, J.B. head-direction cells recorded from the postsubiculum in freely moving rats .1. Description and quantitative-analysis. *Journal of Neuroscience* **10**, 420-435 (1990).

86. Terrazas, A.*, et al.* Self-motion and the hippocampal spatial metric. *Journal of Neuroscience* **25**, 8085-8096 (2005).

87. Tolman, E.C. Cognitive maps in rats and men. *Psychological Review* **55**, 189-208 (1948).

88. Tsodyks, M.V., Skaggs, W.E., Sejnowski, T.J. & McNaughton, B.L. Population dynamics and theta rhythm phase precession of hippocampal place cell firing: A spiking neuron model. *Hippocampus* **6**, 271-280 (1996).

89. Vanderwo.Ch. Hippocampal electrical acitvity and voluntary movement in rat. *Electroencephalography and Clinical Neurophysiology* **26**, 407-& (1969).

90. Vanderwolf, C.H., Leung, L.W.S. & Cooley, r.k. pathways through cingulate, neocortice and entorhinal cortice mediate atropine-resistant hippocampal rhythmical slow activity. *Brain Research* **347**, 58-73 (1985).

91. Whitlock, J.R. & Derdikman, D. Head direction maps remain stable despite grid map fragmentation. *Frontiers in Neural Circuits* **6**, 10 (2012).

92. Wilson, M.A. & McNaughton, B.L. dynamics of the hippocampal ensemble code for space. *Science* **261**, 1055-1058 (1993).

93. Winson, J. Patterns of hippocampal theta rhythm in freely moving RAT. *Electroencephalography and Clinical Neurophysiology* **36**, 291-301 (1974).

94. Witter, M.P., Amaral, D.G. Hippocampal formation. The Rat Nervous System. G. Paxinos. Amsterdam, Elsevier: 635-704 (2004).

95. Witter, M.P., Griffioen, A.W., Jorritsmabyham, B. & Krijnen, J.L.M. entorhinal projections to the hippocampal ca1 region in the rat - an underestimated pathway. *Neuroscience Letters* **85**, 193-198 (1988).

96. Witter, M.P.*, et al.* Cortico-hippocampal communication by way of parallel parahippocampal-subicular pathways. *Hippocampus* **10**, 398-410 (2000).

97. Witter, M.P., Wouterlood, F.G., Naber, P.A. & Van Haeften, T. Anatomical organization of the parahippocampal-hippocampal network. *Parahippocampal Region: Implications for Neurological and Psychiatric Diseases* **911**, 1-24 (2000).

98. Witter, M.P. The perforant path: projections from the entorhinal cortex to the dentate gyrus. *Dentate Gyrus: a Comphrehensive Guide to Structure, Function, and Clinical Implications* **163**, 43-61 (2007).

99. Yoganarasimha, D., Rao, G. & Knierim, J.J. Lateral entorhinal neurons are not spatially selective in cue-rich environments. *Hippocampus* **21**, 1363-1374 (2011).

100. Zilli, E.A. & Hasselmo, M.E. Coupled Noisy Spiking Neurons as Velocity-Controlled Oscillators in a Model of Grid Cell Spatial Firing. *Journal of Neuroscience* **30**, 13850-13860 (2010).

101. Zilli, E.A., Yoshida, M., Tahvildari, B., Giocomo, L.M. & Hasselmo, M.E. Evaluation of the Oscillatory Interference Model of Grid Cell Firing through Analysis and Measured Period Variance of Some Biological Oscillators. *Plos Computational Biology* **5**, 16 (2009).

102. Zilli, E.A. Models of grid cell spatial firing published 2005-2011. *Frontiers in Neural Circuits* **6** (2012).

Appendix A: Cresyl Violet Staining Protocol

CRESYLVIOLET

Perfusion:

Perfuse first with isotonic saline (0.9%) and then with fixative solution (4% formaldehyde) Keep the brain on formaldehyde for at least one week before it's cut.

Cutting:

Freeze the brain and cut it on a cryostat. (Own procedure). The slices is mounted directly on gelatin – treated glass. Let them dry over night before they are stained.

Staining:

Leave the sections in distilled water for 2 min.
Dehydrate sections by dipping them 10 times in each of the baths: 70-, 80-, 90-, 100-, 100-, and 100% ethanol.
Leave the sections in Xylene for 2 min. for clearing
Rehydrate sections by dipping them 10 times in 100-, 100-, 100-, 90-, 80-, and 70% ethanol.
Leave the sections in acetic acid for 5 min.
Rinse quickly in running water.
Leave the sections in Cresylviolet solution for 6-8 min. (Depends how old the staining solution is) Put it on a shaker and leave it in darkness.
Leave the sections in a bath of running cold water until all redundant color is washed off.
Put the sections in acetic acid in a couple of seconds while you shake it carefully in the handle.
Move the sections over in a bath of cold running water, and leave it until all redundant color is washed off.
Repeat step 9 and 10 until the brain slices have a nice bright color with good contrast.
Dehydrate sections (see step 2)
Leave the sections in Xylene for clearing. (They kan be left in Xylene for max. a couple of hours, and a minimum of 5 min.)
Coverslip directly from Xylene bath. Use Eukitt as mounting medium.

Solutions:

Isotonic saline:

9g NaCl in 1L of distilled water

Ethanol:

- 70%: 700ml 96% ethanol mixed with 260ml distilled water
- 80%: 500ml 96% ethanol mixed with 100ml distilled water
- 90%: 800ml 96% ethanol mixed with 50ml distilled water

Acetic acid:

Ad 2,5ml concentrated acetic acid to 500ml of 70% ethanol.

Cresylviolet solution:

0,5g of Cresylviolet (Sigma) is dissolved in 500ml of distilled water. Leave it on a magnet stirrer at 50°C for 2 hrs. Keep it dark. Filter the solution on to a dark colored bottle. Store in room temperature, dark (It crystallizes in the light).

Appendix B: The Correlation between Speed and Acceleration

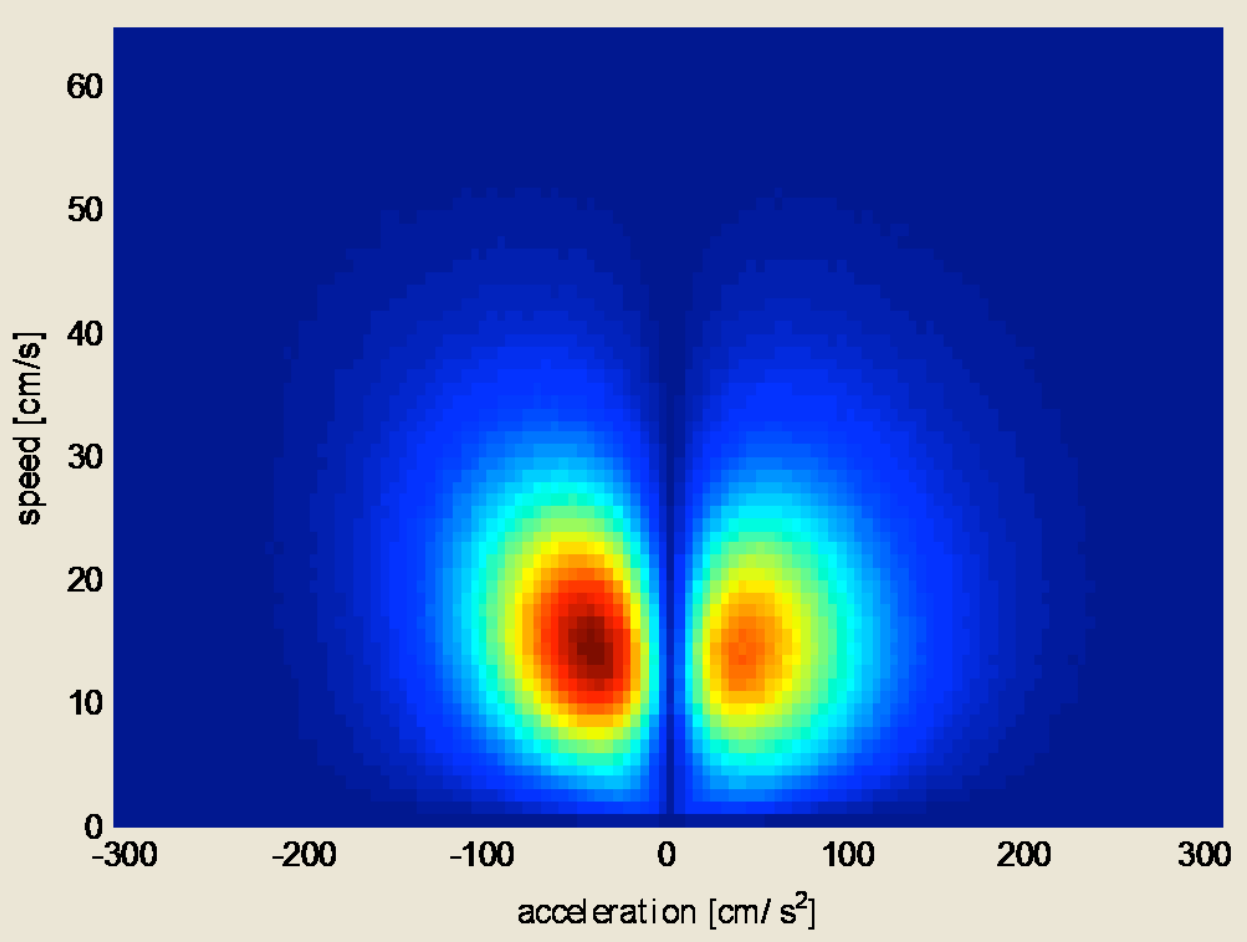

Supplemental Figure: Histogram of the amount of time that three rats spent at a range of speeds and the amount of acceleration for the given speeds. There is a very small amount of time spent at any speed while the acceleration is zero. This exemplifies the tight correlation between speed and acceleration. With the majority of the speeds containing an acceleration component, it becomes difficult to dissociate the two in order to extract any conclusion about the relationship between only speed and the theta frequency using the open field. These data have been compiled across hundreds of sessions for three rats (provided by Kropff)

Appendix C: The Power Spectral Analysis of a typical Cart Session

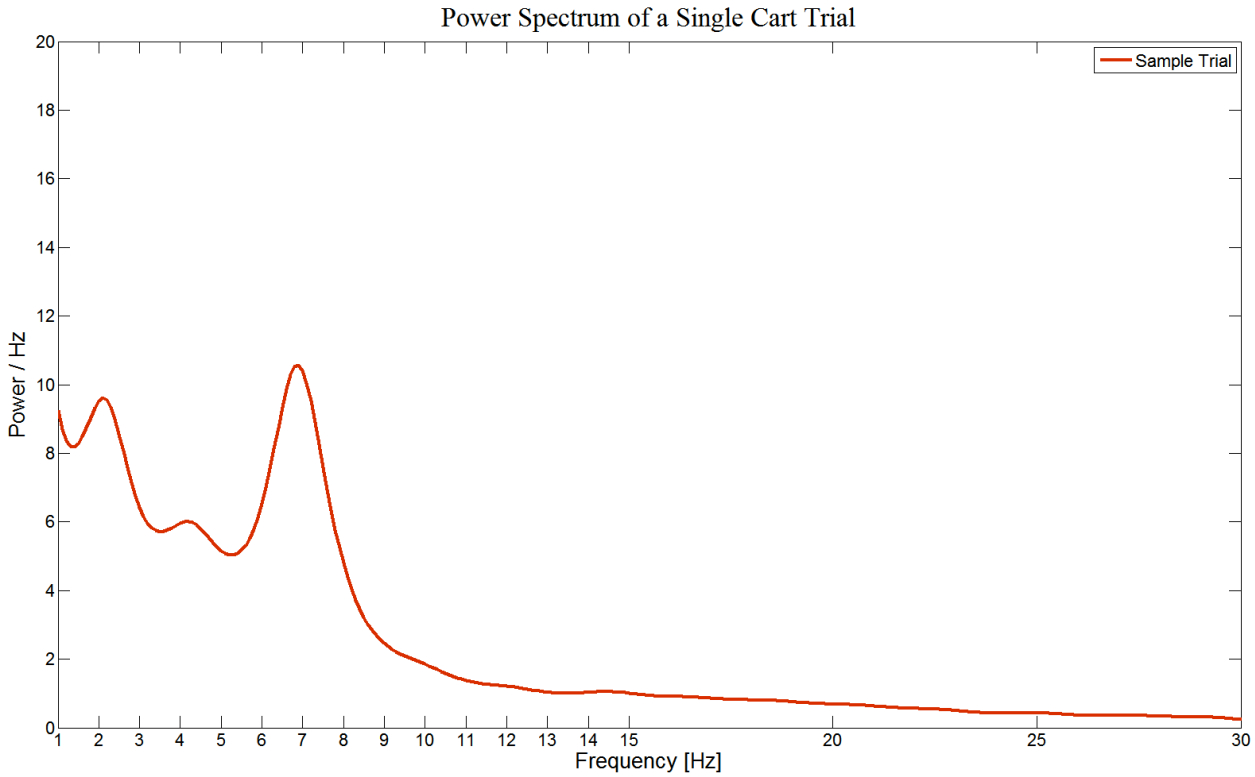

Supplemental Figure: Power Spectrum of a typical cart session. This plot shows the strongest point in the theta and delta ranges. Notice the peaks within the lower theta (7-8Hz), upper delta (4Hz) and lower delta (2-3Hz).